# Forschungszentrum Jülich



Institut für Chemie und Dynamik der Geosphäre 2: Chemie der Belasteten Atmosphäre

# Environmental Simulation Facility to Calibrate Airborne Ozone and Humidity Sensors

Herman G.J. Smit Wolfgang Sträter Manfred Helten Dieter Kley



# Environmental Simulation Facility to Calibrate Airborne Ozone and Humidity Sensors

Herman G.J. Smit Manfred Helten Wolfgang Sträter Dieter Kley

Berichte des Forschungszentrums Jülich ; 3796 ISSN 0944-2952 Institut für Chemie und Dynamik der Geosphäre 2: Chemie der Belasteten Atmosphäre Jül-3796

Zu beziehen durch: Forschungszentrum Jülich GmbH  $\cdot$  Zentralbibliothek D-52425 Jülich  $\cdot$  Bundesrepublik Deutschland

02461/61-6102 · Telefax: 02461/61-6103 · e-mail: zb-publikation@fz-juelich.de

# Environmental Simulation Facility to Calibrate Airborne Ozone and Humidity Sensors

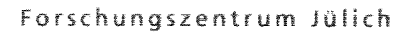
Herman G.J. Smit
Wolfgang Sträter
Manfred Helten
Dieter Kley

Institut für Chemie und Dynamik der Geosphäre 2:

Chemie der Belasteten Atmosphäre, Forschungszentrum Jülich GmbH, Germany

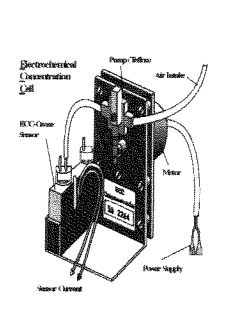
# Facility to Calibrate Airborne Ozone and Humidity Sensors



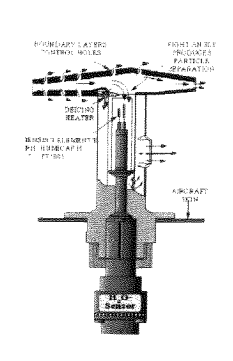


















## Correspondence:

Herman G.J. Smit Forschungszentrum Jülich Institut für Chemie der Belasteten Atmosphäre (ICG-2) D-52425 Jülich, Germany

Tel.: (+)-49-2461-613290 Fax.: (+)-49-2461-615346 E-mail: h.smit@fz-juelich.de .

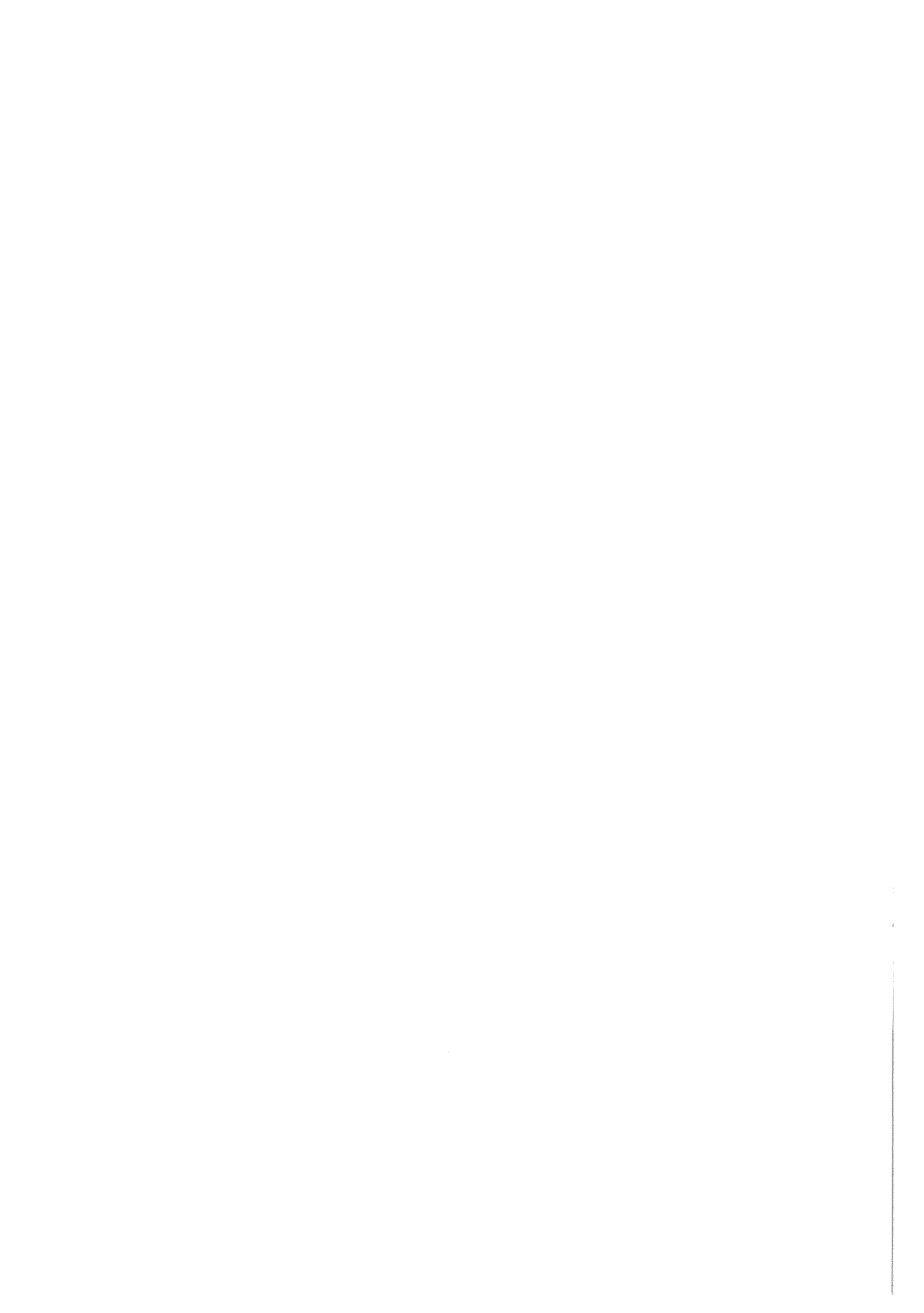
### **Summary**

The Environmental Simulation Facility established at the Forschungszentrum Jülich (FZJ) is designed to investigate the performance of different types of balloon borne ozone sensors as well as air borne humidity sensors to measure the vertical distribution of atmospheric ozone and water vapor, respectively. Key component of the facility is a temperature and pressure controlled simulation chamber with a test room volume of about 500 liter (80x80x80 cm) whereby pressure as well as temperature can be dynamically regulated between 5 and 1000 hPa and between 200 and 300 K (-2K/min  $\leq$  rate  $\leq$  +2K/min) respectively. The volume mixing ratio of ozone can be dynamically regulated between 5 and 10000 ppbv up to a simulation altitude of about 35 km. The relative humidity in the chamber can be varied from about 95% down to 2% over a temperature range between +30°C and -70°C and pressure range between 1000 and 100 hPa. Ozone and humidity sensing devices can be calibrated against accurate reference instruments. A fast response dual beam UV-photometer serves as ozone reference. For the calibration of the water vapor sensors a dew point hygrometer is used for lower/middle tropospheric humidity conditions, while for middle/upper tropospheric conditions a Lyman (α) fluorescence hygrometer serves as reference. The entire simulation process is computer controlled to provide reproducible conditions with respect to pressure, temperature, ozone concentration and humidity.

Since 1994 the chamber is used for the regular (monthly) calibration of water vapor sensing devices which are flown aboard 5 civil "in-service" aircraft (Airbus-A340) within the frame of the European project MOZAIC (Measurement of Ozone and Water Vapor on Airbus In-Service Aircraft) for automatic monitoring of the water vapor distribution in the troposphere. The facility is also established as World Calibration Facility for Ozone Sondes (WCFOS) as part of the Global Atmosphere Watch (GAW) program of the World Meteorological Organization (WMO). In the scope of this frame work several intercomparison experiments, JOSIE (=Jülich Ozone Sonde Intercomparison Experiment), were conducted to assess the performance of the major types of ozone sondes used within the global network of ozone sounding stations. Furthermore, the facility serves as platform to investigate the performance of new developed airborne sensing devices.

## **Table of Contents**

Sun	ımary		V	
1	Intro	oduction	tion of the state	
2 En		vironmental Simulation Facility		
	2.1	Set Up of the Facility	3	
	2.2	Environmental Simulation Chamber	3	
	2.3	Ozone Reference : Dual Beam UV-Photometer	5	
	2.4	Ozone Profile Simulation	8	
	2.5	Humidity Reference Instruments	11	
		2.5.1 Lyman alpha Resonance Fluorescence Hygrometer	11	
		2.5.2 Dew Point Hygrometer	13	
	2.6	Humidity Profile Simulation	15	
	2.7	Data Acquisition System	17	
3.	World Calibration Facility for Ozone Sondes (WCFOS)			
	3.1	Introduction	18	
	3.2	Simulation of Ozone Soundings	19	
4.	Facil	lity for the Calibration of MOZAIC-Humidity Devices	24	
	4.1	Introduction	24	
	4.2	Calibration of MHD	25	
5.	. Concluding Remarks			
Ackı	Acknowledgments			
References			30	



# 1 Introduction

Water vapor and ozone are of crucial importance in both, climate and chemistry of our Earth's atmosphere. As most important greenhouse gas water vapor and in a minor sense ozone play a dominating role in determining climate whereby particularly the radiative feedback of clouds is of great importance. In addition atmospheric water vapor acts as engine of atmospheric dynamics. As chemical substances ozone and water vapor are strongly involved in the chemical oxidation capacity of the atmosphere [Thompson, 1994]. Climate and chemistry of the atmosphere are strongly linked to each other. Climatic changes will influence the chemistry and vice versa. Ozone and water vapor play a key role in the interaction between the chemistry and climate of the atmosphere [Ramanathan et al., 1987]. Long term changes of ozone and water vapor can have a climatic impact on our earth system [IPCC (=Intergovernmental Panel on Climate Change)-report 1994, 1995]

At present there are large deficiencies in the knowledge of the global distribution of ozone and water vapor on spatial as well as temporal scale, particularly in the upper troposphere and lower stratosphere. In order to make reliable predictions of the potential climatic change caused by changes of ozone and water vapor there is a strong need for accurate measurements of the spatial and temporal distribution of tropospheric and stratospheric ozone and water vapor in both hemispheres. Particularly, there is an urgent need for improved data quality for ozone [WMO Scientific Assessment of Ozone Depletion 1998, 1999] as well as for water vapor measurements [IPCC-report 1994, 1995]. This can be achieved by calibration or comparison of the sensing devices with accurate reference instruments.

The environmental simulation facility at the Forschungszentrum Jülich (FZJ) enables control of pressure, temperature, ozone and water vapor concentration. Under realistic atmospheric conditions the airborne ozone or water vapor sensing devices can be compared to accurate reference instruments. A fast response dual beam UV-photometer serves as ozone reference. For the calibration of the water vapor sensors a dew point is used for lower/middle tropospheric water vapor conditions, while for middle/upper tropospheric conditions a Lyman ( $\alpha$ ) fluorescence hygrometer serves as reference.

Since 1996 the facility is established as World Calibration Facility for Ozone Sondes (=WCFOS): a facility for quality assurance of ozone sondes used in the GAW [Global Atmosphere Watch, 1993] program of the WMO (World Meteorological Organization) focusing on ozone sonde precision, accuracy and long term stability [WMO-report No. 104, 1995]. In 1996 a WMO sponsored international intercomparison experiment of ozone sondes, JOSIE = Jülich Ozone Intercomparison Experiment, was conducted at the facility. The aim was to assess the performance of the major types of ozone sondes that are used in the global network of sounding stations [Smit et al., 1998-A & -B].

An important task of the facility since 1994 is the regular (monthly) calibration of water vapor sensing devices which are flown aboard 5 civil "in-service" aircraft (Airbus-A340) within the frame of the European project MOZAIC (Measurement of Ozone and Water Vapor on Airbus In-Service Aircraft) for automatic monitoring tropospheric water vapor, particularly in the middle/upper part of the troposphere. The facility is also used to characterize humidity sensing devices deployed on radiosondes. Further, the facility is a platform to investigate the performance of new developed airborne sensing devices.

In this technical report the major components of the facility are described in detail. In addition, the experimental set up of the ozone sounding simulation in the scope of the WCFOS as well as the typical set up for the calibration of the humidity sensing device used in the MOZAIC program are presented.

# **2** Environmental Simulation Facility

# 2.1 Set Up of the Facility

The environmental simulation facility consists of the following major components:

- I. Temperature and pressure controlled vacuum chamber as environmental simulation chamber (ESC).
- II. Fast response dual beam UV-photometer (OPM) as ozone reference.
- III. Ozone profile simulator (OPS) to simulate dynamically atmospheric ozone profiles
- IV. Lyman alpha fluorescence hygrometer (LFH) as water vapor reference
- V. Humidity profile simulator (HPS) to simulate quasi static humidity levels
- VI. Computer controlled data acquisition system (DAS) for automatic control of the simulation process.

#### 2.2 Environmental Simulation Chamber

The environmental simulation chamber shown in Figure 1 is a temperature controlled vacuum chamber made from stainless steel with a test room volume of about 500 liter (80x80x80 cm) whereby pressure as well as temperature can be dynamically regulated between 5 and 1000 hPa and between 190 and 300 K (-2K/min  $\leq$  rate  $\leq$  +2K/min) respectively.

#### Pressure control:

Evacuation of the chamber is done by 2 scroll pumps (Edwards, Type XDS10) with a pumping capacity of  $20 \text{ m}^3$ /hr at pressures between 5 and 1000 hPa. The pressure inside the simulation chamber is measured with three capacitive manometers: 1-1000 hPa, 0-100 hPa and 0.1-12.5 hPa respectively with an accuracy better than  $\pm 0.5 \%$  of indicated readings. The pressure in the chamber is regulated by the use of a stepper motor controlled exhaust valve (MKS, type 252) between chamber and vacuum pumps in conjunction with secondary air supply. The prescribed pressure versus time profile of the simulation of the sounding can be set by the computer controlled data acquisition system with a resolution of about 0.25 hPa. The actual pressure is recorded with a resolution of about 0.025 % of the full range of the indicated pressure transducer.

#### Temperature control:

The temperature of the walls (incl. door) of the test room and the temperature of the air inside the test room are controlled separately. Temperature regulation is achieved by cooling through expansion of a compressed refrigerant in a heat exchanger and fine regulation by electrical resistance heating. Refrigeration is provided by a two stage refrigerating machine compressor with a total cooling power of about 20 KW at 20 °C and an electrical heating power of about 50 KW. Process control of the different temperatures is done with dual mode regulator circuits which can be set by the computer controlled data

acquisition system (temperature resolution  $\approx 1$  K at temperature range 185 - 440 K). The actual temperatures of the walls (incl. door) and the air inside the test room are monitored with platinum resistance (Pt100) thermometers and recorded at a precision of about +/-0.06 K. Isothermally operated, the temperatures of the air as well as the wall inside the test room can be regulated and kept constant to within  $\pm 0.2$  K.

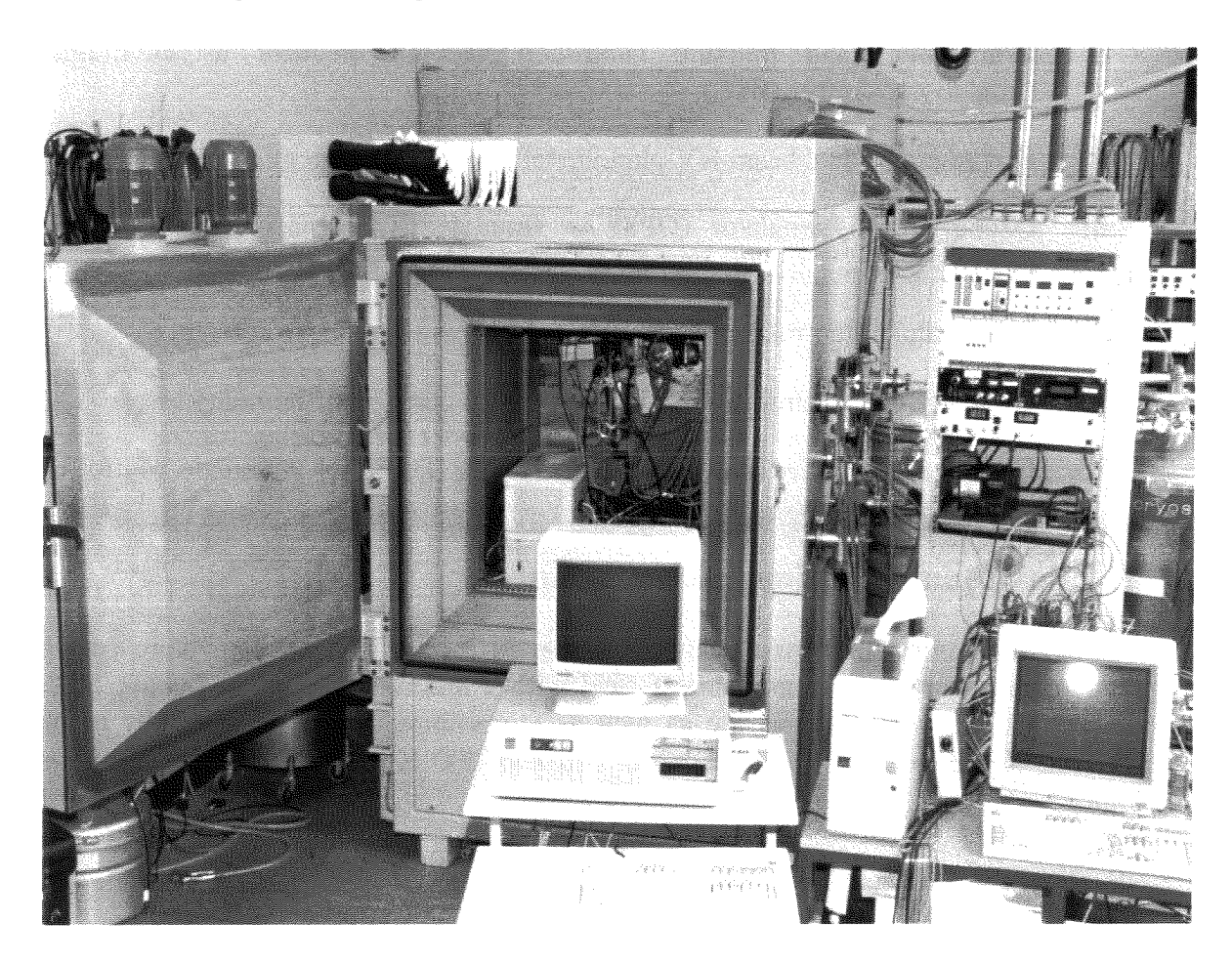
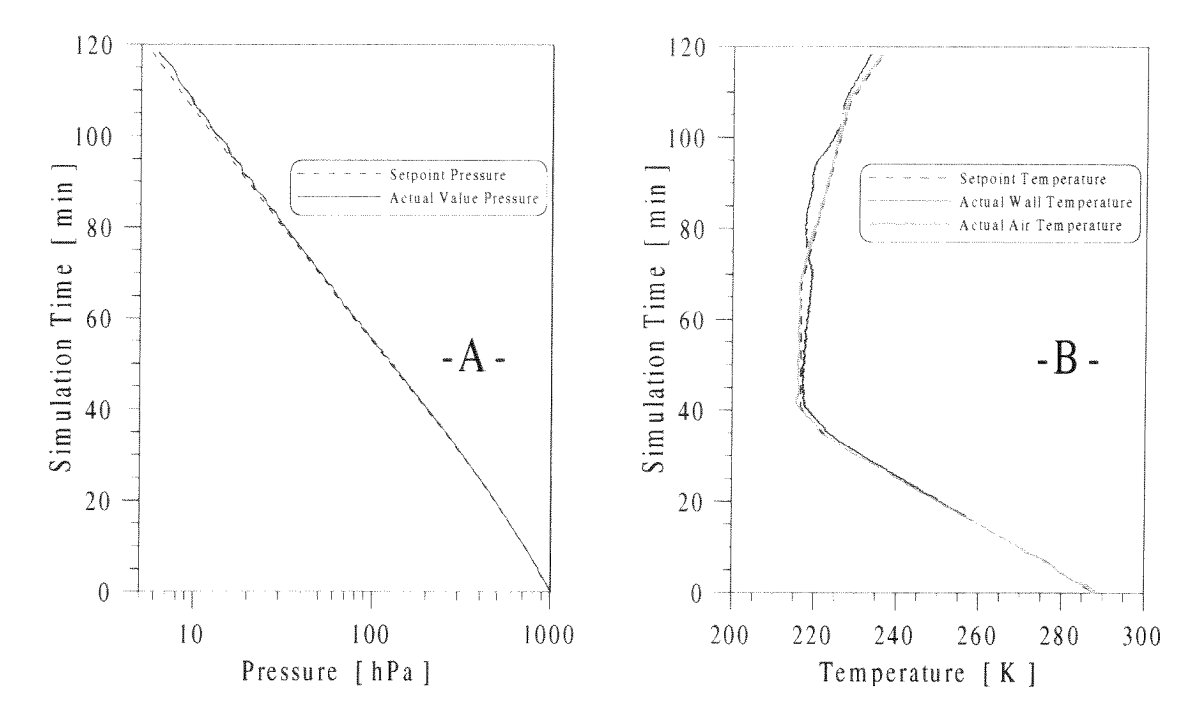


Figure 1: Environmental Simulation Chamber (ESC) at Research Centre Jülich (ICG-2)

Examples of a pressure and a temperature simulation versus time at a balloon ascent velocity of 5 m/s and according typical mid-latitudinal conditions [US-Standard Atmosphere, 1976] are displayed in the Figures 2-A and 2-B respectively. The actual temperature of the (inner) walls of the test room tracks the prescribed temperature profile very well, while the actual temperature of the air inside the test room deviates from the prescribed profile at pressures below 100 hPa. This deviation is due to the fact that at air pressures below 50 hPa heat exchange by forced convection is progressively more ineffective such that thermalization of the air within the test room is limited to heat exchange by thermal radiation of the inner walls of the test room. In addition, more detailed air temperature measurements made at several locations within the test room have shown that at pressures below 100 hPa the test room air temperature show spatial inhomogenities of about 1 K at 100 hPa, 2 K at 50 hPa and 5 K below 25 hPa.



**Figure 2:** Simulation of pressure profile (panel A) and temperature profile of wall and air (panel B) inside the test room of the simulation chamber as a function of the simulation time corresponding to a balloon ascent velocity of 5 m/s. Prescribed profiles are presented by broken lines, while actual observed profiles by solid lines.

#### 2.3 Ozone Reference: Dual Beam UV-Photometer

As ozone reference serves a fast response dual-beam UV-absorption photometer, developed by *Proffitt et al.* [1983] for the use on stratospheric balloons. The instrument has previously flown at several times during BOIC missions in 1983/1984 [Hilsenrath et al. 1986]. A scheme of the instrument is shown in Figure 3.

The instrument has two identical UV-absorption chambers (40 cm long and constructed from Teflon tubing), each alternating between reference mode (ozone free by scrubber) and sample mode. A four port valve alternates the scrubbed air between the two chambers, such that one chamber is in null mode while the other chamber is in sample mode or vice versa. The principle of the instrument of measuring the concentration of ozone in the air sample is based on the spectroscopic UV-absorption measurement of ozone at 254 nm wavelength in the sample chamber according Beer-Lambert absorption law:

$$Ln\left(\frac{I_t}{I_o}\right) = -L \cdot \sigma_{O_3} \cdot C_S$$
 [2-1]

where and  $I_o$  (= zero mode) and  $I_t$  (=sample mode) are the lamp intensities at the detector when the chamber contains the sampled gas with and without removal of the ozone. L is the length of the absorption chamber,  $\sigma_{O3}$  is the molecular absorption cross section of ozone at  $\lambda$ =254 nm, and  $C_S$  is the average concentration of ozone in the absorption chamber. Since L and  $\sigma_{O3}$  are well known quantities, the transmittance R of the absorption

chamber from the observed signal frequencies of the photo detector in sample and zero mode,  $F_{sample}$  and  $F_{zero}$  respectively is determined by

$$\mathbf{R} = \left(\frac{\mathbf{I_t}}{\mathbf{I_o}}\right) = \frac{\mathbf{F_{sample}}}{\mathbf{F_{zero}}}$$
 [2-2]

yields Cs

$$C_{S} = \frac{-Ln(R)}{L \cdot \sigma_{O_{3}}}$$
 [2-3]

The dual beam feature cancels the effects of lamp intensity fluctuations while the mode alternation compensates for mechanical changes and also provides continuous measurements. Details of the data reduction method are described by *Proffitt et al.* (1983). The instrument is an absolute measuring device with a fast response time of about 1 second at a sampling volume flow rate of about 8 l/min.

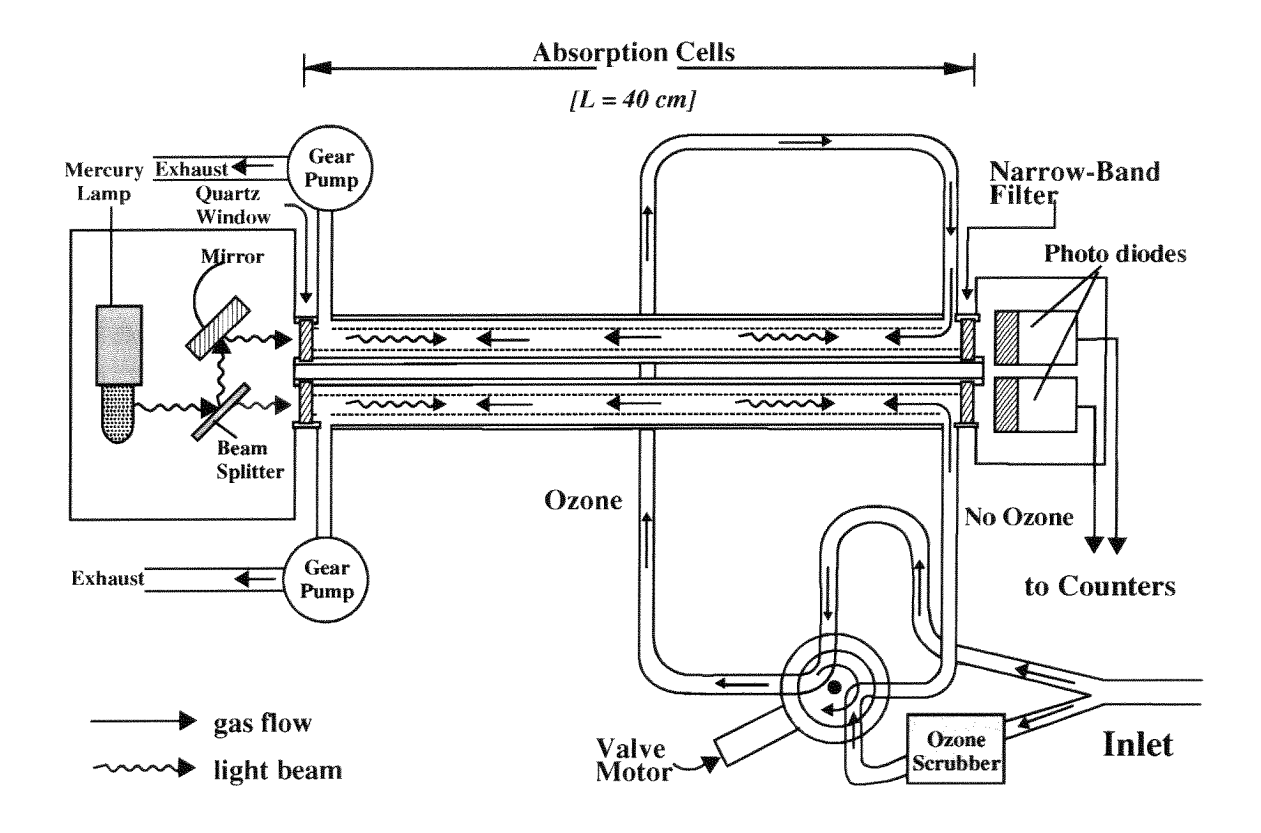
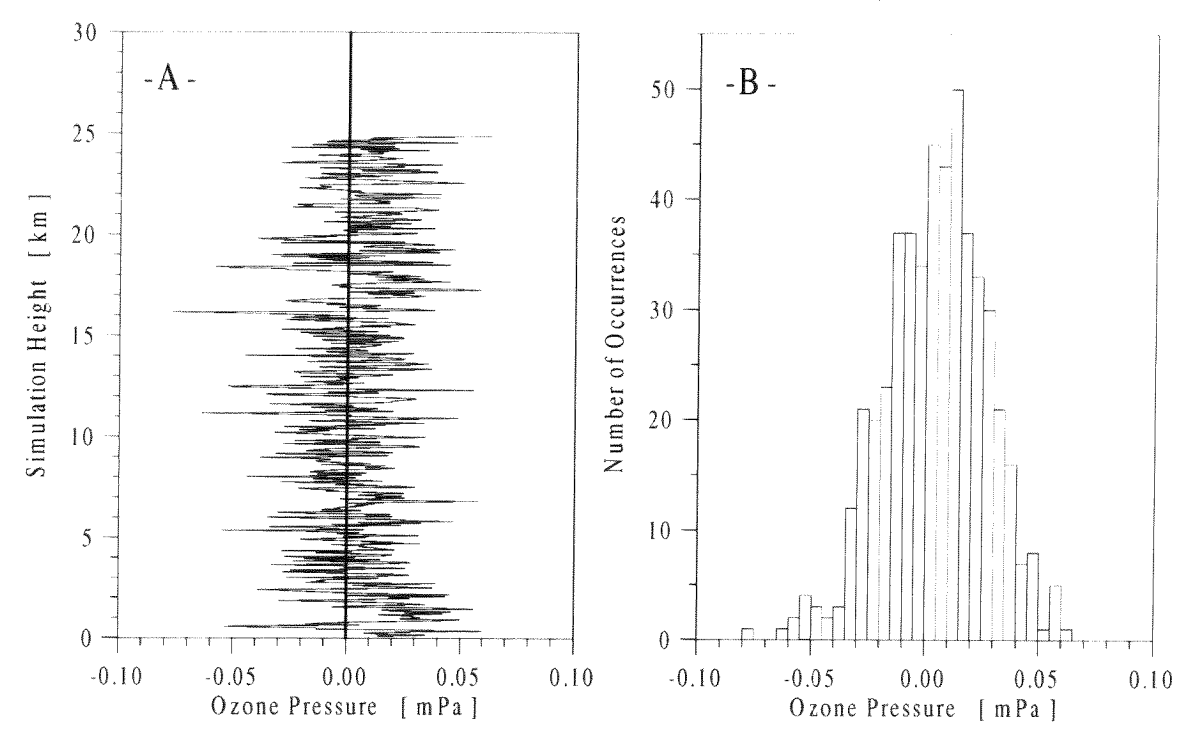


Figure 3: Scheme of the dual beam UV-absorption photometer [Proffitt et al., 1983]

The ozone UV-Photometer is installed in a separate vacuum vessel which is connected to the simulation chamber such that the UV-photometer is operated at the same pressure conditions as inside the test room. The air sample intake of the photometer is connected via a Teflon tube to the manifold of the ozone profile simulator which is located in the center of the test room.

The minimum detectable ozone concentrations are determined by the inherent noise of the photometer. Figure 4-A shows the fluctuations of the background of the photometer as a function of altitude. The results are presented as ozone equivalent and were obtained from flight simulations in the chamber by feeding the photometer with ozone free air. It is seen that the fluctuations of the background of the photometer are rather constant for altitudes between surface and 25 km. It is seen from Figure 4-B that the statistical distribution of the background of the photometer is closely following Gaussian statistics with a mean background of 0.005 mPa and a standard deviation of  $\pm$  0.025 mPa. The minimum detectable levels of ozone of the photometer are around 0.025 mPa ( $\cong$ 0.6x10<sup>10</sup> molecules/cm³ of O³) with a virtually zero( $\leq$ 0.005 mPa of O³) background level. The precision of the ozone measurement made by the UV-photometer as reference is estimated to be better than  $\pm$ 0.025 mPa of O³ ( $\cong$ 0.6x10<sup>10</sup> O³ molecules/cm³).



**Figure 4:** Background of dual beam ozone UV-photometer as ozone pressure equivalent. Left panel A: Background as a function of altitude. Right panel B: Statistical distribution (histogram) of background.

The absolute accuracy of the photometer is primarily determined by the uncertainty of the absorption path length, the uncertainty of the molecular absorption cross section of ozone and eventual losses of O<sub>3</sub> within the instrument. The path length of 40.2 cm is known to better than ±0.2% while the molecular absorption cross section of ozone of 1.147x10<sup>-17</sup> molecules/cm<sup>2</sup> [Vigroux, 1953] is considered to have an uncertainty smaller than ±1.5% [Proffitt et al., 1983]. Ozone losses inside the instrument can in principle occur on the wall surfaces. In general relative wall losses of trace constituents in laminar flows varies as P<sup>-2/3</sup> where P is the total gas pressure [Levich, 1962]. Based on laboratory measurements Proffitt estimated relative losses of ozone within the instrument to be smaller than 1% for air pressures at 25 hPa, 2% at 15 hPa and 4% at 5 hPa. Therefore, it is obvious that, for air pressures corresponding to tropospheric and lower stratospheric conditions up to 25 km altitude, ozone losses within the photometer are negligible small and do not significantly affect the accuracy of the instrument. The overall accuracy of the ozone measurements

made by the UV-Photometer as reference is therefore better than  $\pm 2\%$  for simulated altitudes up to 25 km while it declines to  $\pm 3.5\%$  at 35 km altitude.

#### 2.4 Ozone Profile Simulation

In order to simulate vertical ozone profiles dynamically in time as well as to achieve reproducible ozone concentrations, a separate gas mixing system is installed to provide up to 4 ozone sensors plus UV-photometer (OPM) with regulated ozone concentrations. The scheme of the so called ozone profile simulator (OPS) is presented in Figure 5.

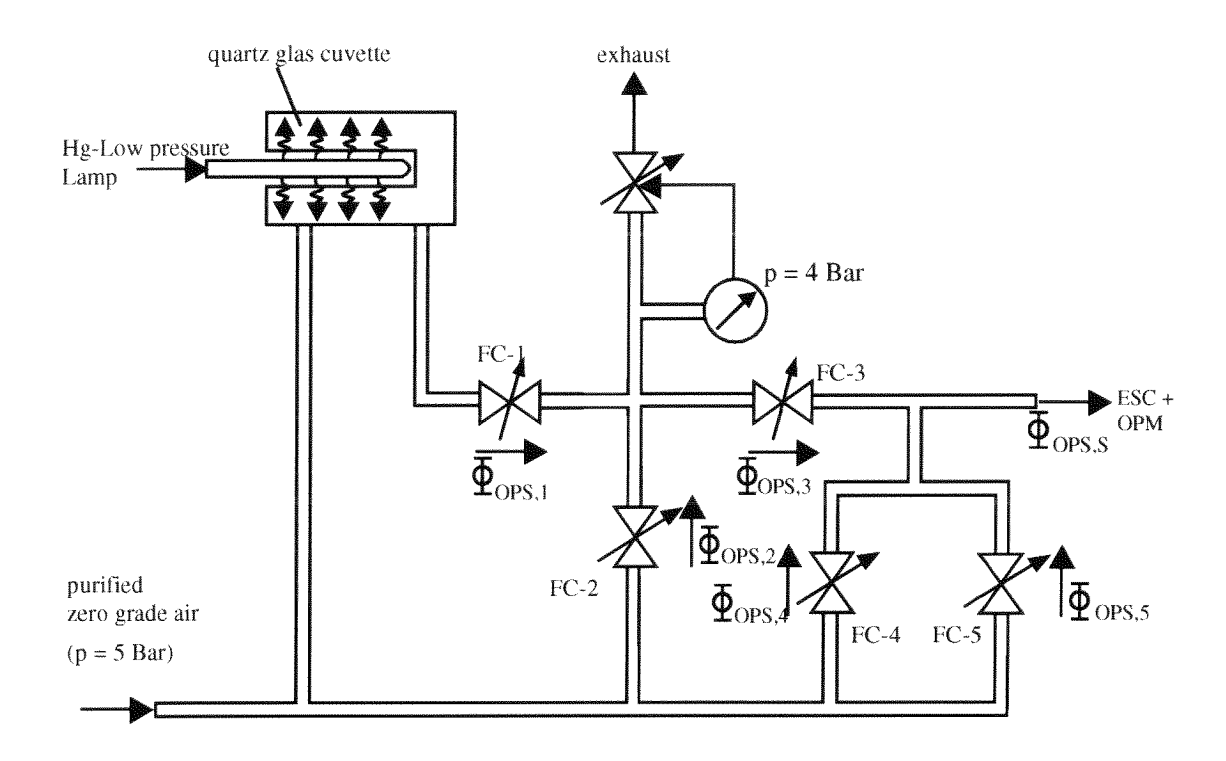


Figure 5: Scheme of the set up of the ozone profile simulator (OPS)

Ozone is photolytically generated by UV-irradiation in a zero grade air flow through a quartz glass (Suprasil) tube using a low pressure Hg-lamp. Via the photodissociation of oxygen molecules at a wavelength of 185 nm and the additional reaction of oxygen atoms with oxygen molecules ozone is formed at high concentration levels of 0.1-2~% in a constant air mass flow of  $20~\text{cm}^3/\text{min}$ , pressurized at 4.0 Bar, through the quartz glass cell (volume  $\approx 40~\text{cm}^3$ ). In order to vary the mixing ratio of ozone between 10 and 10000 ppbv the highly ozone concentrated air flow is dynamically diluted by a multiple staged mixing with zero grade air flows. All air flows are regulated by mass flow controllers.

At a first dilution stage the high concentrate ozone/air flow  $\Phi_{OPS,1}$  is mixed with zero grade air flow  $\Phi_{OPS,2}$  (0-2000 cm³/min) at 2.0 Bar total pressure, the excess vented by a valve. A part of the resulting diluted ozone air flow, $\Phi_{OPS,3}$  (0-2000 cm³/min) , is fed into a second dilution stage where it is mixed with two zero grade air flows,  $\Phi_{OPS,4}$  (0-2000 cm³/min) and  $\Phi_{OPS,5}$  (0-10000 cm³/min), at test room pressure conditions. The resulting air flow,  $\Phi_{OPS,8}$  ( $\Phi_{OPS,8}$ = $\Phi_{OPS,3}$  +  $\Phi_{OPS,4}$  +  $\Phi_{OPS,5}$ ), with diluted ozone is fed into the manifold, located in the test room of the simulation chamber, to supply the ozone sensors plus UV-

photometer with controlled ozone mixing ratios. The relation between the diluted and undiluted mixing ratio of ozone,  $\chi_{O3,OPS}$  and  $\chi_{O3,UnDil}$  respectively, as a function of the mass flow rates,  $\Phi_{OPS,1}$ ,  $\Phi_{OPS,2}$ ,  $\Phi_{OPS,3}$ ,  $\Phi_{OPS,4}$  and  $\Phi_{OPS,5}$  is given by:

$$\chi_{O_3,OPS} \equiv \frac{\Phi_{OPS,1}}{\Phi_{OPS,1} + \Phi_{OPS,2}} * \frac{\Phi_{OPS,3}}{\Phi_{OPS,3} + \Phi_{OPS,4} + \Phi_{OPS,5}} * \chi_{O_3,UnDil}$$
[2-4]

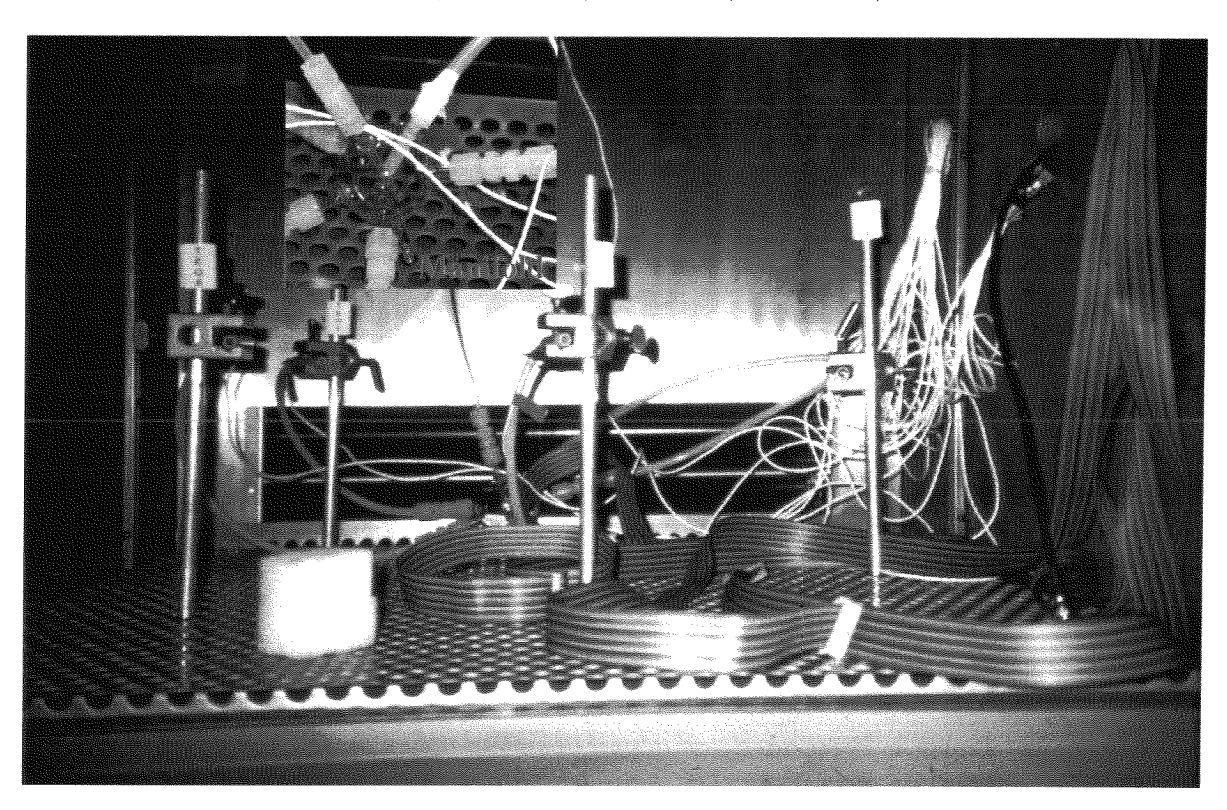


**Figure 6:** View inside testroom of environmental simulation chamber with setup to test 4 ozone sondes. Detailed view of manifold at outlet of ozone profile simulator (OPS) to supply 4 ozone sondes plus UV-photometer with controlled ozone concentrations mixed in air.

The manifold shown in Figure 6 consists of a spherical glass vessel with a volume of about  $150~\rm cm^3$  with radially arranged connections to the individual ozone sensors and the UV-photometer with the inlet of the simulated ozone air flow  $\Phi_{OPS,S}$  being in the center of the manifold. Excess amounts of air are exhausted via an additional tube into the test room such that the manifold is kept to the test-room pressure conditions in order to prevent the ozone sensors from over-pressure effects. The latter effects would increase the mass flow rate through the ozone sensors and thus yield an overestimate of the actual ozone concentrations measured by the test ozone-sensors.

The volume flow rate of the simulated ozone air flow  $\Phi_{OPS,S}$  is kept constant within a range of 10-12 l/min which is sufficient to provide four ozone sensors (maximum 4 x 250 ml/min) and the photometer (maximum 8 l/min) yet limiting the exhaust flow into the test room such avoiding over-pressure in the manifold as well as a large excess of air flow which would affect the pressure regulation of the chamber.

During the entire simulation the undiluted ozone mixing ratio  $\chi_{O3,UnDil}$  is kept constant by keeping the conditions for the ozone production such as pressure, UV-light and mass flow

within the quartz tube at constant levels. Just prior to each simulation  $\chi_{O3,UnDil}$  is adjusted to typical prescribed surface pressure, temperature and ozone conditions.

On the basis of the prescribed simulation profiles of ozone mixing ratio, pressure and temperature plus the experimental boundary conditions of a constant mixing ratio of ozone in the undiluted flow  $\Phi_{OPS,1}$  and a constant sample volume flow rate  $\Phi_{OPS,S}$  the mass flow rates of  $\Phi_{OPS,2},\,\Phi_{OPS,3}$ ,  $\Phi_{OPS,4}$  and  $\Phi_{OPS,5}$  are calculated according equation 2-4, optimized and set by computer control.

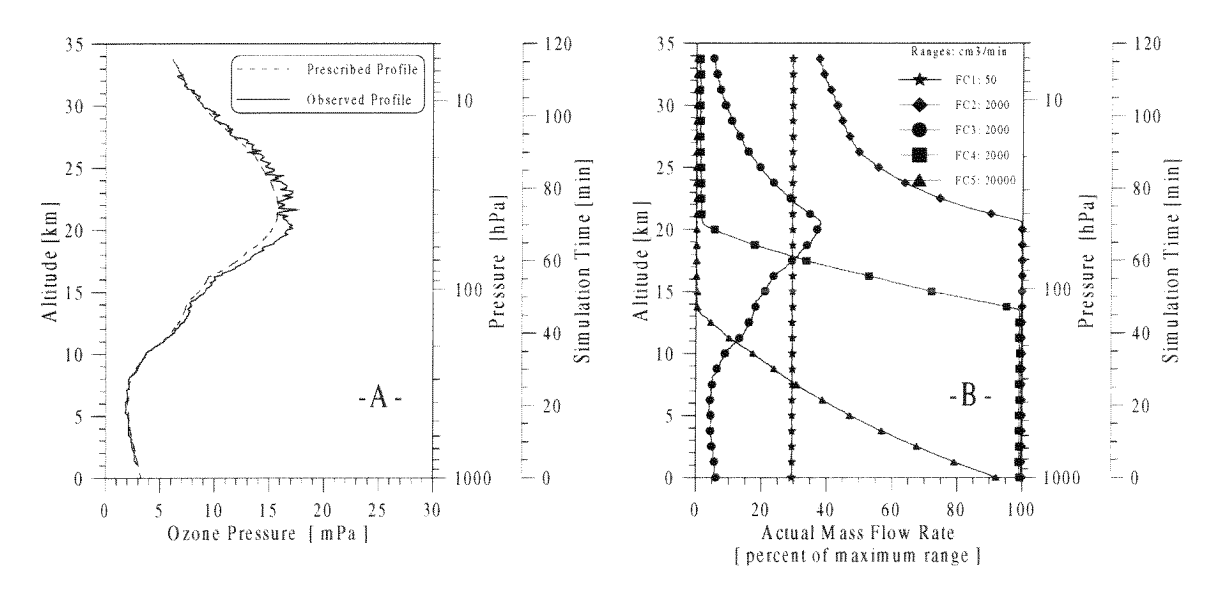


**Figure 7:** Panel A: Prescribed and actual observed ozone profile simulated at typical mid latitude conditions according US-Standard Atmosphere (1976) for 40-50°N with a tropopause height of about 12 km. Panel B: Actual mass flow rates of the ozone profile simulator (OPS) as function of the simulated altitude.

An example of the simulation of a vertical ozone profile is presented in Figure 7 which shows a vertical profile of the prescribed ozone partial pressure as calculated from the experimental conditions (equation 2-4) as well as the actual profile of ozone as measured with the UV-photometer. It is seen that the actual simulated ozone profile tracks the prescribed profile very well, within an agreement of 5-10 %, in the tropospheric as well as in the stratospheric part of the simulation. The combined operation of the five mass flow controllers (FC-1,2,3,4&5) during the simulation of a vertical profile of ozone is illustrated in Figure 7-B showing the actual mass flow rates,  $\Phi_{OPS,1}$ ,  $\Phi_{OPS,2}$ ,  $\Phi_{OPS,3}$ ,  $\Phi_{OPS,4}$  and  $\Phi_{OPS,5}$  as a function of the actual simulated height. A sensitivity analysis of equation 2-4 in combination with the actual mass flow rates, presented in Figure 7-B, have shown that the simulated ozone mixing ratio is most sensitive by the settings of the flow controllers FC-3, -4 & -5 of the second dilution stage. Regarding the limited accuracy and reproducibility of mass flow controllers if operated in the lower part of their measuring range it is clear that in the stratospheric part where the mass flows are small the simulated profile of ozone is becoming sensitive to small variations of the different flows. Therefore, it is likely that the fluctuations of ozone observed by the photometer in the stratospheric part (see Figure 7-B) are caused by the small variations of the air flows through FC-3, FC-4 and particularly FC-5.

# 2.5 Humidity Reference Instruments

# 2.5.1 Lyman alpha Resonance Fluorescence Hygrometer

For the water vapor measurements a Lyman-alpha fluorescence hygrometer (LFH) [Kley et al., 1978], is installed in the simulation chamber as reference instrument. The principle of the instrument is based on the absorption measurement of  $H_2O$  at the Lyman-alpha line of hydrogen ( $\lambda$ =121.6 nm) in combination with the detection of the OH ( $\lambda$ =310 nm) fluorescence which is produced by photolysis of  $H_2O$  at the Lyman-alpha radiation. This combination of detection techniques makes a two beam absorption instrument unnecessary and allows for measurements of extremely low  $H_2O$  concentrations.

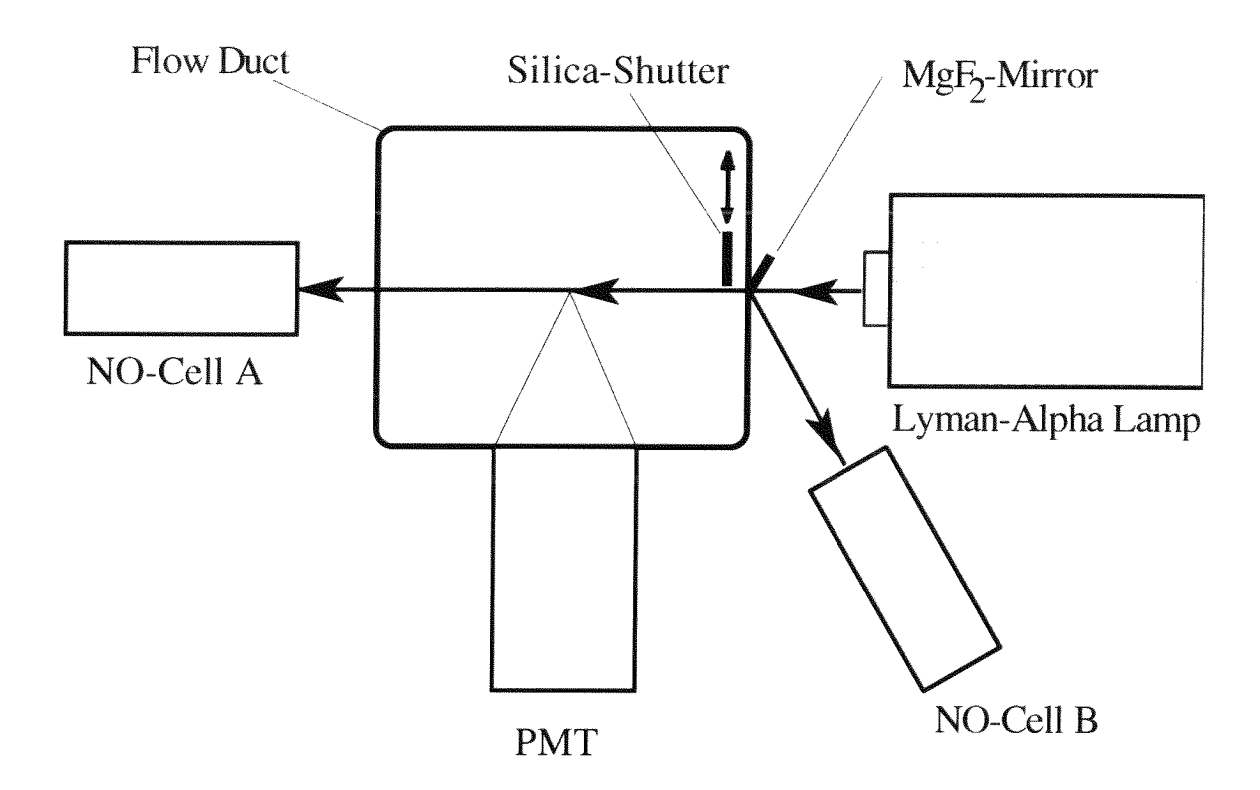


**Figure 8:** Cross section of Lyman-alpha fluorescence hygrometer perpendicular to the flow channel of the instrument. The radiation of the lamp enters the air stream channel through a pinhole and is partly reflected by a MgF<sub>2</sub> plate to cell B. After traversing the flow duct the light beam leaves it through a pinhole and reaches cell B. The scattered radiation inside the flow duct is detected by the photomultiplier looking perpendicular to the light beam in the duct.

Figure 8 shows a cross section of the instrument, perpendicular to the flow duct. In a rigid ground plate an air flow duct is mounted. The radiation from the Lyman-alpha lamp enters the flow duct through a hole and runs through a second hole to the NO cell A. This establishes the main absorption path  $x_A$  of the instrument. For a secondary light path  $(x_B)$  a small part of the radiation is reflected by a MgF<sub>2</sub> plate to a second NO cell B. Light path  $x_B$  is shorter than  $x_A$ .

Absorption Mode

The Lyman-alpha intensities  $I_A$  and  $I_B$  at cell A respectively B in this set-up are then given by

$$\mathbf{I}_{\mathbf{A}} = \mathbf{I}_{0} \cdot \mathbf{EXP} \left[ -\left( \mathbf{\sigma}_{02} \cdot \left[ \mathbf{O}_{2} \right] + \mathbf{\sigma}_{H20} \cdot \left[ \mathbf{H}_{2} \mathbf{O} \right] \right) \cdot \mathbf{x}_{\mathbf{A}} \right]$$
[2-5]

$$\mathbf{I}_{\mathbf{B}} = \mathbf{I}_{0} \cdot \mathbf{C} \cdot \mathbf{EXP} \left[ -\left( \mathbf{\sigma}_{\mathbf{O}2} \cdot \left[ \mathbf{O}_{2} \right] + \mathbf{\sigma}_{\mathbf{H}2\mathbf{O}} \cdot \left[ \mathbf{H}_{2}\mathbf{O} \right] \right) \cdot \mathbf{x}_{\mathbf{B}} \right]$$
[2-6]

where  $I_0$  the lamp intensity,  $[O_2]$  and  $[H_2O]$  the concentrations of oxygen and water, and  $\sigma_{O2}$  and  $\sigma_{H2O}$  the corresponding absorption cross sections. C is a constant, which accounts for the different beam geometry, reflectivity of the MgF<sub>2</sub> mirror and sensitivity of NO cell B relative to NO cell A.

If factor C is known, the water vapor concentration can be determined by

$$[\mathbf{H}_{2}\mathbf{O}] = -\left\{ \frac{\mathbf{L}\mathbf{N} \begin{pmatrix} \mathbf{I}_{\mathbf{A}} \cdot \mathbf{C} / \\ \mathbf{I}_{\mathbf{B}} \end{pmatrix}}{\mathbf{x}_{\mathbf{A}} - \mathbf{x}_{\mathbf{B}}} + \sigma_{\mathbf{O}2} \cdot [\mathbf{O}_{2}] \right\} / \sigma_{\mathbf{H}2\mathbf{O}}.$$
 [2-7]

Under conditions of very low water vapor concentration (  $[H_2O] \approx 0$ ), the factor C is obtained from

$$C = \left[\frac{I_B}{I_A}\right]_{[H_2O]=0} \cdot EXP(\sigma_{O2} \cdot [O_2] \cdot (x_A - x_B)).$$
 [2-8]

A first estimate of C can therefore be taken from the measurements of the lowest water vapor concentrations measured during an experiment. For a precise determination of C also the fluorescence measurement has to be taken into account.

Fluorescence Mode

The Lyman-alpha radiation dissociates H<sub>2</sub>O molecules into OH and H

$$H_2O + hv \Rightarrow OH(A^2\Sigma^+) + H(^2S).$$

One part of the electronically excited OH gives a fluorescence at 310 nm wavelength, while the rest is electronically quenched by  $N_2$  and  $O_2$ 

$$OH(A^2\Sigma^+)$$
  $\Rightarrow$   $OH(X^2\Pi)$  + hv  $(\lambda = 310 \text{ nm})$ 

The 310 nm fluorescence is observed with a photomultiplier mounted in the flow duct at right angle to the direct light beam traversing the flow duct on path A.

The measured fluorescence signal S (after subtraction of the background counting rate) is proportional to the  $H_2O$  volume mixing ratio  $\mu_{H2O}$  for moderate  $H_2O$  concentrations. It is not exactly linearly dependent on  $\mu_{H2O}$ , due to  $Ly(\alpha)$ -light absorption between lamp and fluorescence volume. Therefore the relation for S can be written as

$$S \sim \mu_{H2O} \cdot I_0 \cdot EXP[-(\mu_{H2O} \cdot \sigma_{H2O} + 0.2 \cdot \sigma_{O2}) \cdot [Air] \cdot x_F]$$
 [2-9]

where  $x_F$  is the length of the light path from the lamp to the middle of the fluorescence volume in the flow duct.

The exponential expression describes the "pre-absorption" of Ly( $\alpha$ )-light before it photodissociates H<sub>2</sub>O in the fluorescence volume and gives rise to the OH fluorescence at  $\lambda$ =310 nm. Since the layout of the instrument provides that  $x_B = x_F$ , the pre-absorption is proportional to the signal of cell B and relation 2-9 can be written as

$$\mathbf{S} \sim \mathbf{\mu}_{\mathbf{H2O}} \cdot \mathbf{I}_{\mathbf{B}} \tag{2-10}$$

By dividing the measured fluorescence counting rate through the measured  $I_B$  signal one has effectively linearized the response of the instrument with respect to "pre-absorption" and eliminated any changes due to fluctuations in lamp intensity [*Kley et al.*, 1979]. Thus the corrected counting rate  $S_{corr}$  of the fluorescence can be expressed as

$$S_{corr} \equiv \frac{S}{I_B} = B \cdot \mu_{H2O}$$
 [2-11]

which is now exactly linear in  $\mu_{H2O}$ . Constant B is the sensitivity of the corrected fluorescence count rate. An estimated  $\mu_{H2O}$  can be computed by equation 2-7 with an estimate of constant C.  $S_{corr}$  is linearly correlated with the estimated volume mixing ratio  $\mu_{H2O}$  showing normally also an offset. Using this offset and the slope of the linear regression, the correct C can be computed and B in equation [2-11] can be determined. This is done for each temperature level, at which the calibration procedure is executed. The slope B in equation [2-11] of the final linear regression gives a calibration of the fluorescence count rate for the  $H_2O$  mixing ratio.

The accuracy of the water vapor mixing ratio measurements in the fluorescence mode of the instrument is  $\pm 4\%$ , including random and systematic errors with inclusion of the accuracy of the absorption cross sections for water vapor and oxygen at  $\lambda=121.6$  nm wavelength [Kley, 1984].

# 2.5.2 Dew Point Hygrometer

For humidities larger than 0.5g/kg, i.e. lower tropospheric conditions, an optical condensation dew point hygrometer (General Eastern 1311DR) is used, allowing microprocessor-based control, measurement and display. It incorporates a chilled mirror dew point sensor for measurements in a dew point range of -75°C to +95°C. It is calibrated against dew point standards that are traceable to the U.S. National Institute of Standards and Technology.

The principle of the detection method is the optical observation of a metallic mirror, which can be controlled within a wide range of temperatures by Peltier elements and a resistance heater. The dew layer building up, when the mirror temperature is falling below the dew point temperature, is optically detected and its temperature than held at that temperature and measured with a precise Platinum resistance thermometer, delivering the dew/frost point temperature. The optical detection of the dew layer is done by monitoring the light of a high intensity LED, reflected from the mirror surface, with a photo detector. When the dew layer forms, diffuse reflection leads to an attenuated signal of the photo detector. The specifications of the instrument are shown in Table 1

The air to be monitored is sucked with a stainless steel tube (6 mm  $\varnothing$ ) from the sample flow of the of the Lyman-alpha hygrometer (LFH) into the dew point hygrometer (DPH) by

a small bellows pump with 2 l/min (STP). The tube is electrically heated with a coaxial resistance heater on its full length to avoid memory effects of the wall inside the tube.

Dew Point Range	-75°C to +50°C	
Pressure Range	5 to 1100 hPa	
Input Duct	Heated Stainless Steel Tube	
Humidity Range	0 to 85 % Relative Humidity	
Sample Flow Rate	0.25 to 2.5 l/min	
Accuracy	± 0.2°C	
Precision	± 0.05°C	
Response Time	1,5°C/sec above 0°C	

Table 1: Specifications of dew point mirror hygrometer General Eastern D1311R

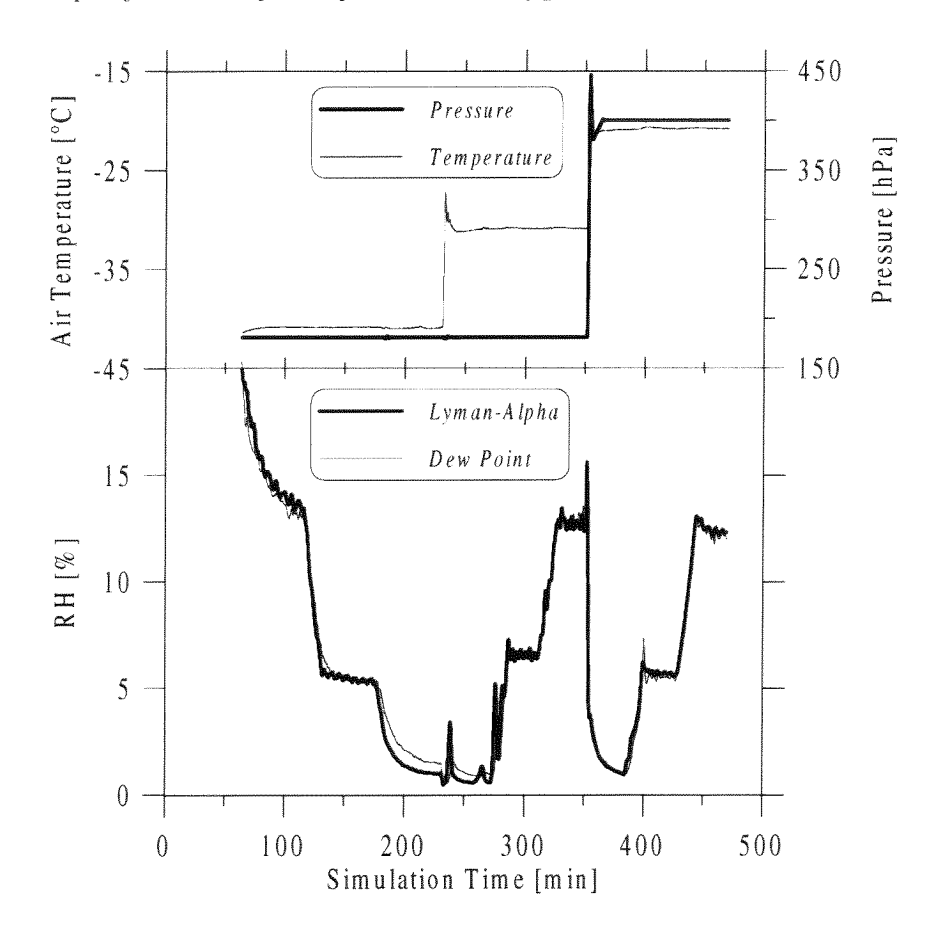


Figure 9: Set points of air temperature, wall temperature, and relative humidity with resulting measured dew-point temperature (dew point hygrometer) and relative humidity (Lyman-alpha hygrometer) as function of simulation time.

Figure 9 gives an impression of the instrument performance in comparison with the Lyman-alpha hygrometer measurement in the simulation chamber together with pressure and temperature as function of the simulation time. For temperatures below -20°C there is a positive offset of the dew point hygrometer in the order of 1 % RH compared with the Lyman-alpha. For relative humidities above 4 % the reading of the dew point hygrometer is close to that of the Lyman-alpha for all temperatures. At steep changes of the humidity the response time of the dew point instrument is long, increasing with decreasing temperature, and needs some minutes of recovery. At relative humidity levels below 4 % and fast changes of humidity the dew point hygrometer's accuracy is not sufficient for calibrations, while at higher humidity levels the relative deviation between dew point hygrometer and Lyman-alpha hygrometer is systematically below 10 % of the reading, provided fast humidity changes are excluded.

# 2.6 Humidity Profile Simulation

Air and wall temperature of the chamber can be regulated independently within certain limits. The relative humidity inside the chamber during a simulation run is defined by the ratio of the actual water vapor pressure and saturated water vapor pressure with respect to the air temperature inside the chamber. The design of the humidity simulation is such that the wall temperature determines the dew (frost) point temperature of the air inside the chamber. This means that the water vapor partial pressure can be lowered by cooling the walls to a temperature lower than the air temperature. Differences between air and wall temperatures up to 25 °C can be reached in the chamber, as long as the air pressure is above 100 hPa.

The water vapor pressure in the chamber can achieve its maximum value corresponding to the water vapor saturation pressure determined by the temperature of the walls, the coldest parts inside the chamber. The relative humidity of the chamber air is therefore defined through

$$\mathbf{RH} = \frac{100 \cdot \mathbf{E}(\mathbf{T}_{\text{Wall}})}{\mathbf{E}(\mathbf{T}_{\text{Air}})}$$
 [2-12]

if saturation with respect to the wall temperature is reached. E is the water vapor saturation pressure in percent,  $T_{Wall}$  and  $T_{Air}$  the absolute temperatures of the chamber air and the walls respectively.

For E(T<sub>Air</sub>) we always use the water vapor saturation pressure over a plane surface of liquid water, since relative humidity with respect to liquid water is the usual measure in the scientific community. E(T) is derived using the *Goff and Gratch* (1946) formulation as recommended by the World Meteorological Organization [WMO-Report No.8, 1983] and adapted to the International Temperature Scale 1990 (ITS-90) [Sonntag, 1994]<sup>1</sup>.

$$E(T) = EXP \left[ \frac{a}{T} + b + c \cdot T + d \cdot T^2 + e \cdot LN(T) \right], \text{ where E is in Pa, T in K.}$$

For liquid water the constants are:

<sup>&</sup>lt;sup>1</sup> The water vapor saturation pressures with respect to a plane surface of liquid water or ice is respectively:

a = -6096.9385, b = 21.2409642, c = -2.711193E-2, d = 1.673952E-5, and e = 2.433502 For ice the constants are:

a = -6024.5282, b = 29.32707, c = 1.0613868E-2, d = -1.3198825E-5, and e = -0.49382577

At a constant air temperature different relative humidities can be set by regulating the wall temperature of the chamber. Figure 10 gives an example of a humidity simulation run at different temperature and humidity levels inside the chamber.

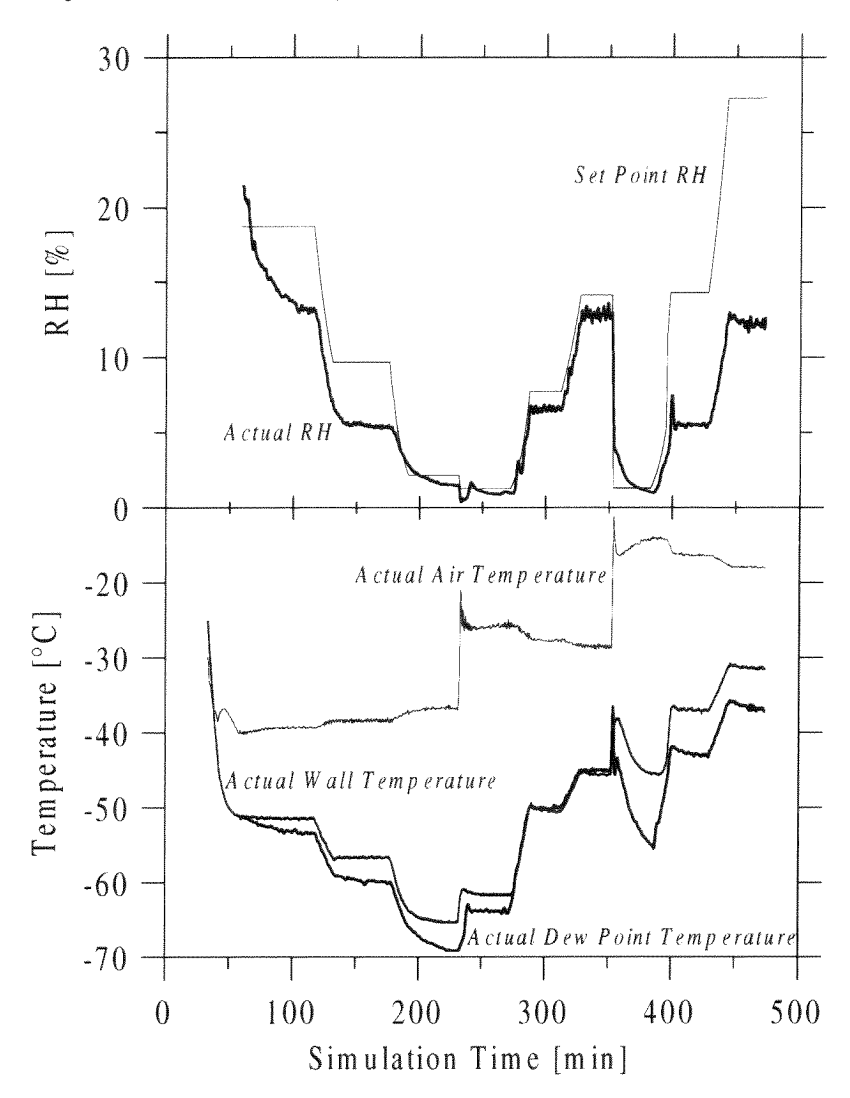


Figure 10: Measurement of RH (by Lyman-alpha fluorescence hygrometer), air temperature, wall temperature, and pressure as function of simulation time during a typical run of the environmental simulation chamber for the calibration of humidity sensors in the MOZAIC project.

In the lower panel the actual air and wall temperatures as a function of the simulation time are shown. The upper panel displays the relative humidity expected from the actual air and wall temperatures and the actual relative humidity measured with the Lyman-alpha hygrometer. At an air temperature of -30°C there is good agreement between actual and expected relative humidity, while at temperatures of -20°C and -40°C the actual humidity is much lower than the expected humidity.

Comparing the actual wall temperature with the actual dew point temperature measured by the dew point hygrometer, it is obvious that the prescribed humidity is higher than what is actually found in chamber air. This water deficiency is most likely caused by inhomogenities of temperatures and adsorption on the surfaces of the walls and the fins of the heat exhanger inside the chamber. This is overcome by the addition of controlled

amounts of water vapor to the air inside the chamber during a simulation run. The necessary addition of water vapor is achieved by injection of moistened air into the chamber, regulated by a software PID-controller which uses the actual wall temperature as set point and compares with the actual dew point temperature measured by the dew point hygrometer.

# 2.7 Data Acquisition System

The entire simulation process is automated by computer control to have reproducible conditions with respect to the simulation process of pressure, temperature, ozone, and humidity versus time as well as with respect to the recording and storage of the large variety of parameters measured during the simulation process. The computer controlled simulation facility enables us to investigate the performance of the different-types of ozone and humidity sensing devices under quasi flight conditions in the troposphere and lower/middle stratosphere up to 35 km altitude. The technical specifications of the simulation facility are summarized in Table 2.

- Test room volume = 500 liter (80x80x80 cm)
- Separate temperature control of wall (inclusive. door) and air inside the test room
- Computer controlled simulation according to "real" atmospheric conditions:
  - a.) Pressure: 5-1000 hPa
    - Separate control of air and wall temperature:  $\Delta T \le 30 \text{ K}$
    - dynamic: Rate =  $\pm 2$  K/min
    - static: Fluctuations <= 0.1-0.2 K
  - c.) Ozone: Mixing Ratio 5-10000 ppbv (0.1-30 mPa)
  - d.) Water Vapor: Dew Point Temperature: 190 300 K
- Ozone Reference:

Dual Beam UV-Photometer [Proffitt et al., 1983]:

- Response: 1 s
- Precision: ±0.025mPa,
- Accuracy:  $\pm 2\%$  (0-25 km),  $\pm 4\%$  (30-35km)
- Water Vapor Reference:

Lyman alpha Fluorescence Hygrometer [ Kley et al., 1978]:

- Response: 1 s
- Precision: ±0.5 %
- Accuracy: ±4%

**Table 2:** Specifications of environmental simulation facility for the calibration of airborne ozone and humidity sensing devices.

# 3 World Calibration Facility for Ozone Sondes (WCFOS)

#### 3.1 Introduction

The state of knowledge regarding long term trends of tropospheric as well as stratospheric ozone is limited due to inadequate global coverage of ozone sounding stations, poor assurance of data continuity and questionable homogeneity of data [WMO-Scientific Assessment of Ozone Depletion 1998: 1999]. Particularly, there is an urgent need for improved data quality which must be achieved by intercalibration and intercomparison of existing ozone sonde types as well as agreement through procedures for data processing and analysis [WMO-report No. 104, 1995, SPARC-IOC-GAW, 1998]. Several previous series of WMO-field intercomparisons where several different types of ozone sondes were simultaneously flown, have been conducted [Attmanspacher et al., 1970, 1981, and Kerr et al., 1994]. However, many questions with regard to the observed instrumental performance of the different ozone sondes were left unanswered. A key shortcoming was that in most intercomparisons no ozone reference standard was simultaneously flown.

Since 1996 the environmental simulation chamber at Forschungszentrum Jülich is established as World Calibration Facility for Ozone Sondes (=WCFOS) of the WMO: a facility for quality assurance of ozone sondes used in GAW/GLONET focusing on ozone sonde precision, accuracy and long term stability. The controlled environment plus the fact that the ozone sonde measurements can be compared to an accurate UV-Photometer as reference [*Proffitt et al.*, 1983, *Smit et al.* 1994] allows to conduct experiments that are designed to address questions which arise from field operation. In 1996 the activities started with the Jülich Ozone Sonde Intercomparison Experiment (JOSIE-1996) which was attended by eight ozone sounding laboratories from seven countries and representing the major types of ozone sondes that are in routine operation in GAW/GLONET [*Smit et al.*, 1998-B].

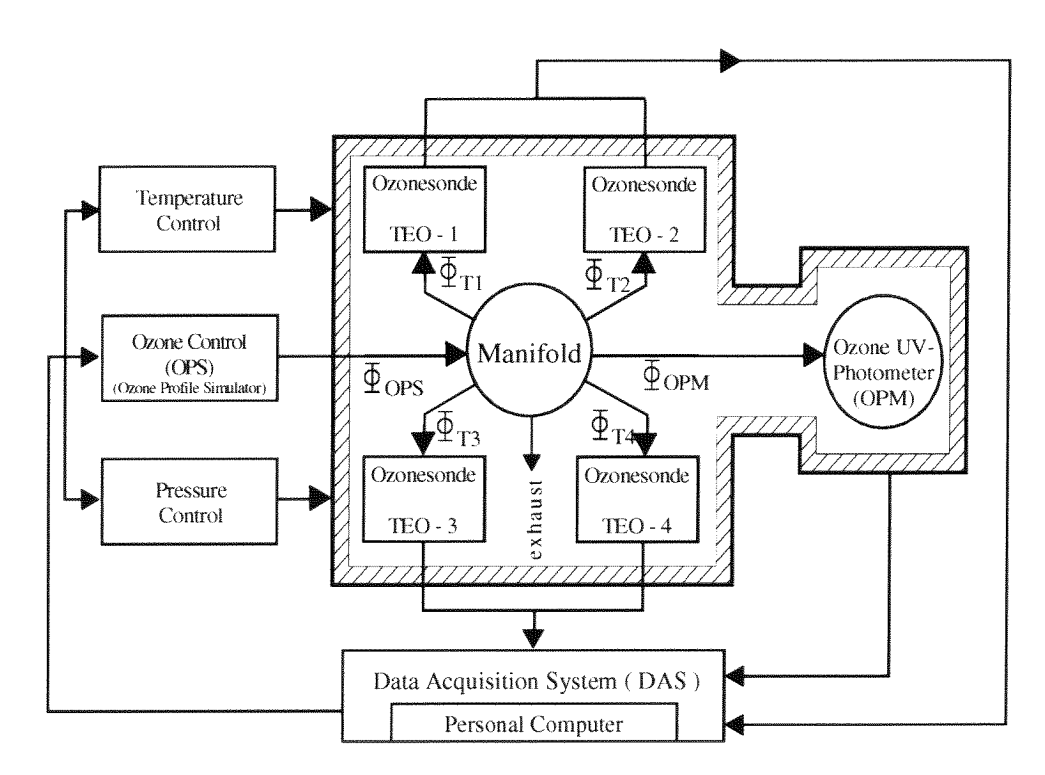


Figure 11: Scheme of the set up of the ozone sounding simulation experiment

# 3.2 Simulation of Ozone Soundings

Ozone sondes are small, lightweight and compact balloon borne instruments, developed for measuring the vertical distribution of atmospheric ozone up to an altitude of about 35-40 km. The ozone sensor is mostly based on an electrochemical method. In Figure 12 the world wide used ECC (=Electrochemical Concentration Cell) ozone sonde, developed by *Komhyr* [1969], is shown.

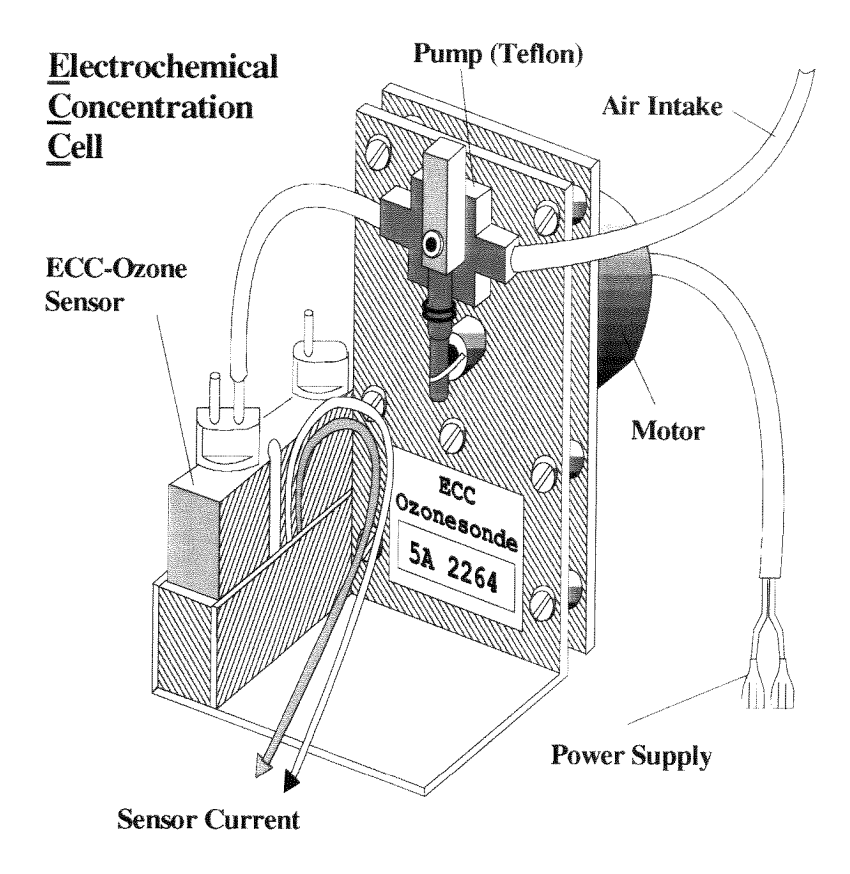


Figure 12: Electrochemical Concentration Cell (ECC, after Komhyr, 1969)

The principle of ozone measurement is thereby mostly based on the titration of ozone in a potassium iodide (KI) sensing solution according the redox reaction:

$$2 \text{ KI} + \text{O}_3 + \text{H}_2\text{O} \longrightarrow \text{I}_2 + \text{O}_2 + 2 \text{ KOH}$$

The amount of generated "free" iodine  $(I_2)$  is measured in electrochemical reaction cell(s). Continuous operation is achieved by a small electrically driven gas sampling pump which forces ambient air through the sensing solution of the electrochemical cell. Transported by the stirring action of the air bubbles, the iodine makes contact with a platinum cathode and is reduced back to iodide ions by the uptake of 2 electrons per molecule of iodine.

$$I_2$$
 + 2e — Pt  $\rightarrow$  2  $I^{-}$  [cathode reaction]

An electrical current proportional to the mass flow rate of ozone through the cell is generated. In principle, this type of electrochemical ozone sensor is an absolute measuring device. By knowing the gas volumetric pumping rate and the gas temperature the measured electrical current is converted to the ozone concentration in the sampled ambient air.

During normal flight operation, ozone sondes are coupled via special interfacing electronics with radiosondes for data transmission and additional measurement of meteorological parameters like pressure, temperature (optional humidity and wind). Total weight of the flight package is about 1 kg which can be flown on weather balloons. The data measured by the sonde is telemetered to the ground station for further data processing.

The experimental set up for the simulation of the vertical ozone soundings in the chamber is shown in Figure 11. Four ozone sondes can be "flown" simultaneously (see Figure 13) and compared to the UV-photometer. One of the major objectives of the experiments is to characterize and to determine precision and accuracy of the ECC-ozone sensor as a function of altitude and ozone level. Particularly the question is addressed in how far the data analysis is affected by procedures like background signal correction and total ozone column normalization.

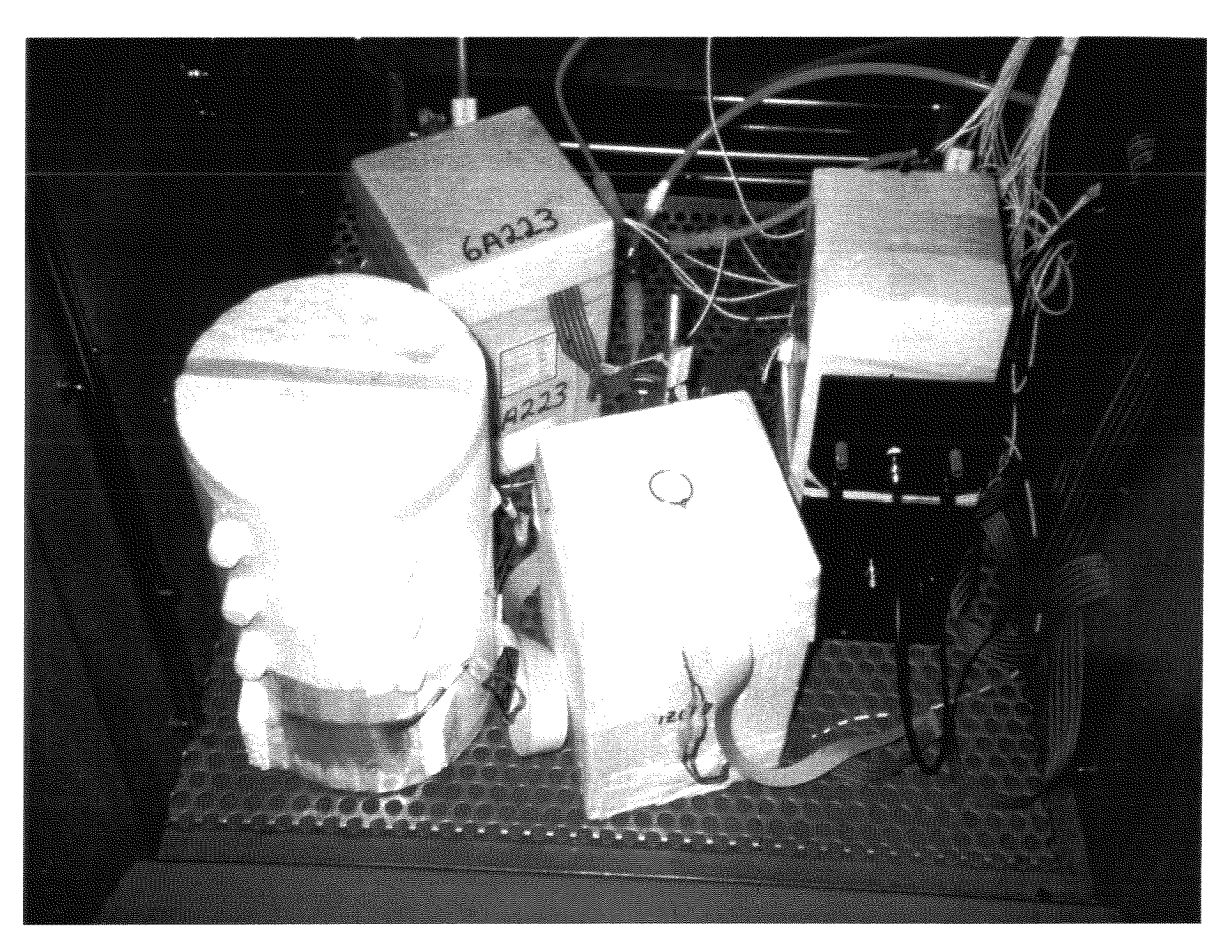


Figure 13: Four different ozone sondes installed in the environmental simulation chamber just prior to a simulation of an ozone sounding during JOSIE-1996

Different types of vertical profiles of pressure, temperature and ozone concentrations can be simulated. Two examples are shown in Figure 14. The first type of profile is a typical mid-latitude profile taken from the US-Standard Atmosphere (1976) for 40-50 °N with a tropopause height of 12 km. The second type of profile relates to typical tropical conditions of high convective activity, high tropopause at 18 km and low tropopause temperature which means extremely low ozone values in the middle and upper troposphere [Kley et al., 1996]. In addition, different types of ozone step functions or zero ozone can be applied in order to investigate the response time and background characteristics of the different ozone sondes.

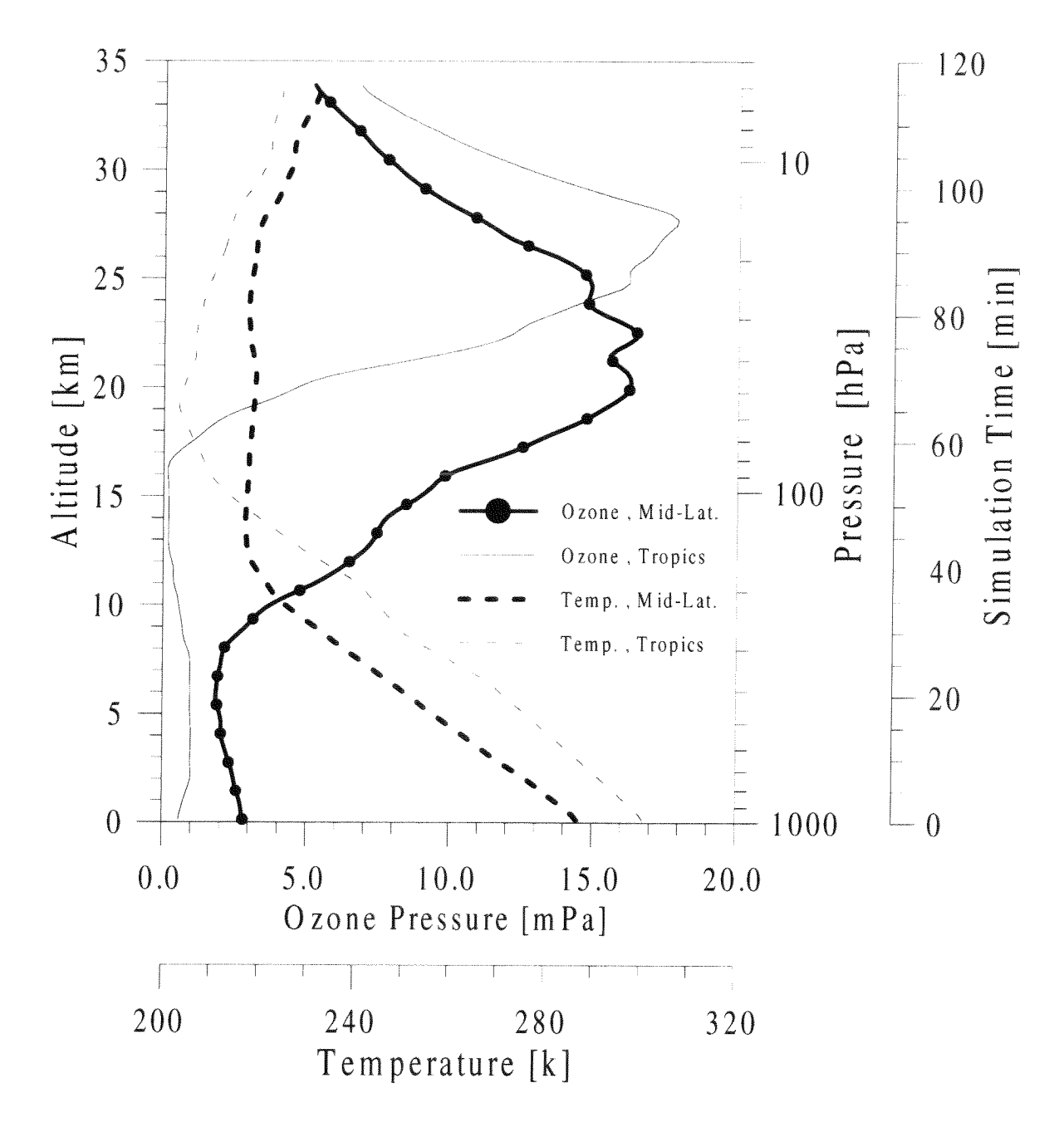


Figure 14: Vertical profiles of the simulation of ozone pressure and temperature at midlatitude and tropical conditions.

To illustrate the performance of the facility for the simulation of ozone soundings some results of a typical mid-latitude and tropical simulation run of four simultaneously "flown" sondes compared to the UV-photometer, which were obtained during JOSIE in 1996, are displayed in the upper and lower diagrams respectively of Figure 15.

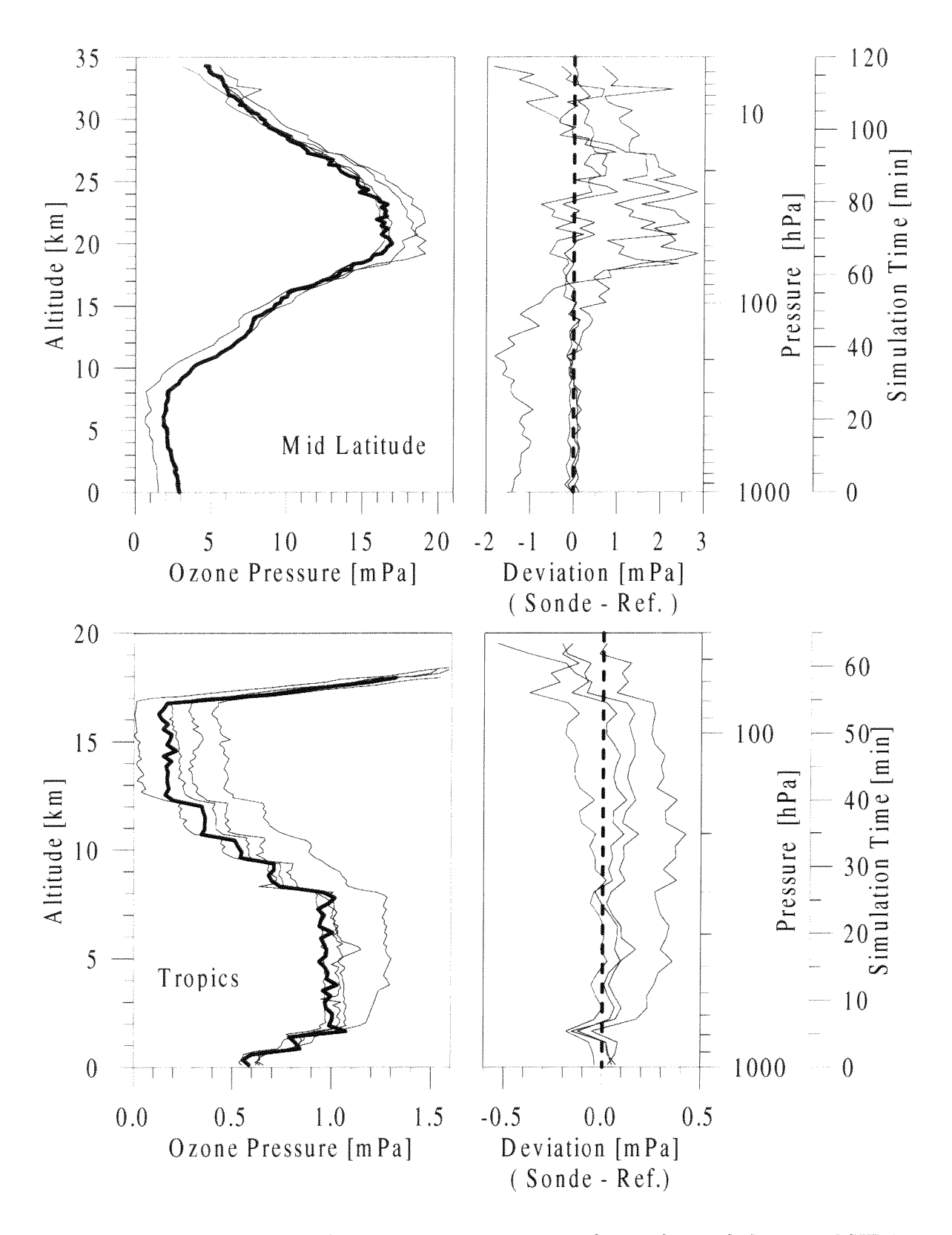


Figure 15: Examples of simulation runs of ozone soundings obtained during JOSIE in 1996. Comparison of four different ozone sondes with the UV-Photometer. Upper panel: Mid latitude conditions, Lower panel: Tropical conditions. Left graphs: Vertical ozone profiles obtained by individual sondes (thin lines) and UV-Photometer (fat line). Right graphs: Deviations of the individual sondes with regard to the readings of the UV-Photometer.

In addition, Figure 16 shows the results of some time response tests of four different ozone sondes when ozone was temporarily set to zero during some simulation runs made during JOSIE.

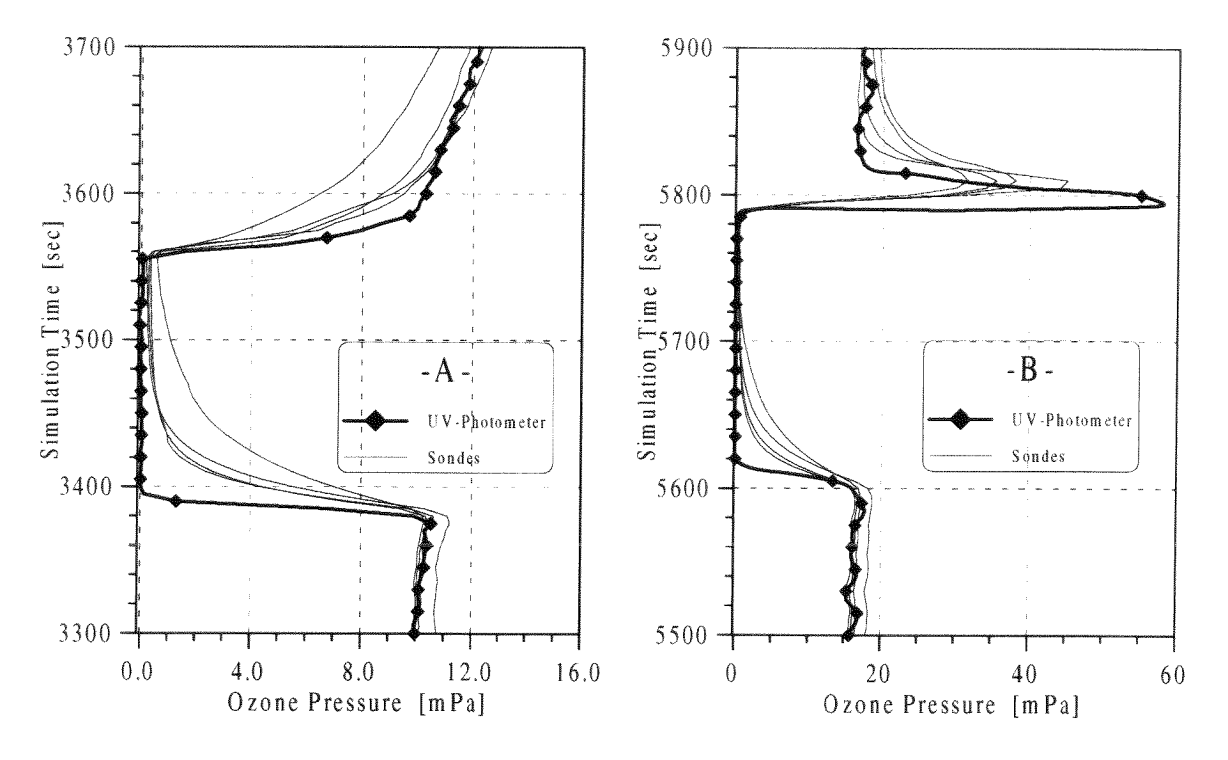


Figure 16: Examples of time responses of different ozone sondes when ozone was temporarily set to zero during the during simulation runs of ozone soundings made during JOSIE in 1996. Comparison of four different ozone sondes (thin lines) with the UV-Photometer (fat line).

The different experiments to simulate ozone soundings brought valuable information about the performance of the different ozone sonde types and the influence of the operating procedures for preparation and data correction on the data quality of ozone soundings. The simulation experiments showed also that there is a need to validate ozone sondes on a routine basis. Ozone sondes have gone through some modifications since they were first manufactured, which adds uncertainty to trend analysis. Routine testing of newly manufactured ozone sondes on a regular basis, following a standard operating procedure (SOP), will help to ensure more confidence in observed trends in the future. A pre-requisite thereby is the standardization of the preparation procedures and data correcting methods in the near future, but also a better and more detailed documentation of the procedures and methods applied in the past at the different long term ozone sounding stations. Therefore, in order to support the assessment of the standardization of preparation procedures of ozone sondes a second international ozone sonde intercomparison experiment (JOSIE-2000) to be conducted in the course of the year 2000 is planned. Pre-experiments sponsored by the WMO, prior to JOSIE-2000, have been performed in 1998 and 1999.

## 4. Facility for the Calibration of MOZAIC-Humidity Devices

#### 4.1 Introduction

Within the MOZAIC <sup>2</sup> project (Measurement of Ozone and Water Vapor by Airbus In Service Aircraft) the large scale distribution of tropospheric water vapor is quasi continuously measured on board five AIRBUS A340 aircraft during in-service flights [Marenco et al., 1998] by use of regularly calibrated humidity sensors (See Figure 17).



Figure 17: Airbus A340 equipped with MOZAIC-Humidity Device. Inlet system mounted at the outside skin of the aircraft close to the cone.

The MOZAIC-Humidity Device (MHD) is a special airborne humidity sensing device (AD-FS2), developed by Aerodata (Braunschweig, Germany) and based on the humidity and temperature transmitter HMP230 of Vaisala (Helsinkin, Finnland). As illustrated in Figure 18 the sensing element itself is a combination of a capacitive relative humidity sensor (Humicap-H, Vaisala) and a Pt100 temperature sensor which has been installed in a Rosemount housing mounted on the outside skin of the aircraft in the vicinity of the nose cone. Relative humidity and temperature are electronically measured by a transmitter unit and fed into the data acquisition system of MOZAIC aboard the A340 aircraft. Before installation in the aircraft and after about 500 hours of flight operation, each MOZAIC-Humidity Device is calibrated in the environmental calibration facility.

<sup>&</sup>lt;sup>2</sup> MOZAIC is supported by EU (European Union) and sponsored by four major European airlines (Air France (1 aircraft), Austrian Airlines (1 aircraft), Lufthansa (2 aircraft) and Sabena (1 aircraft)).

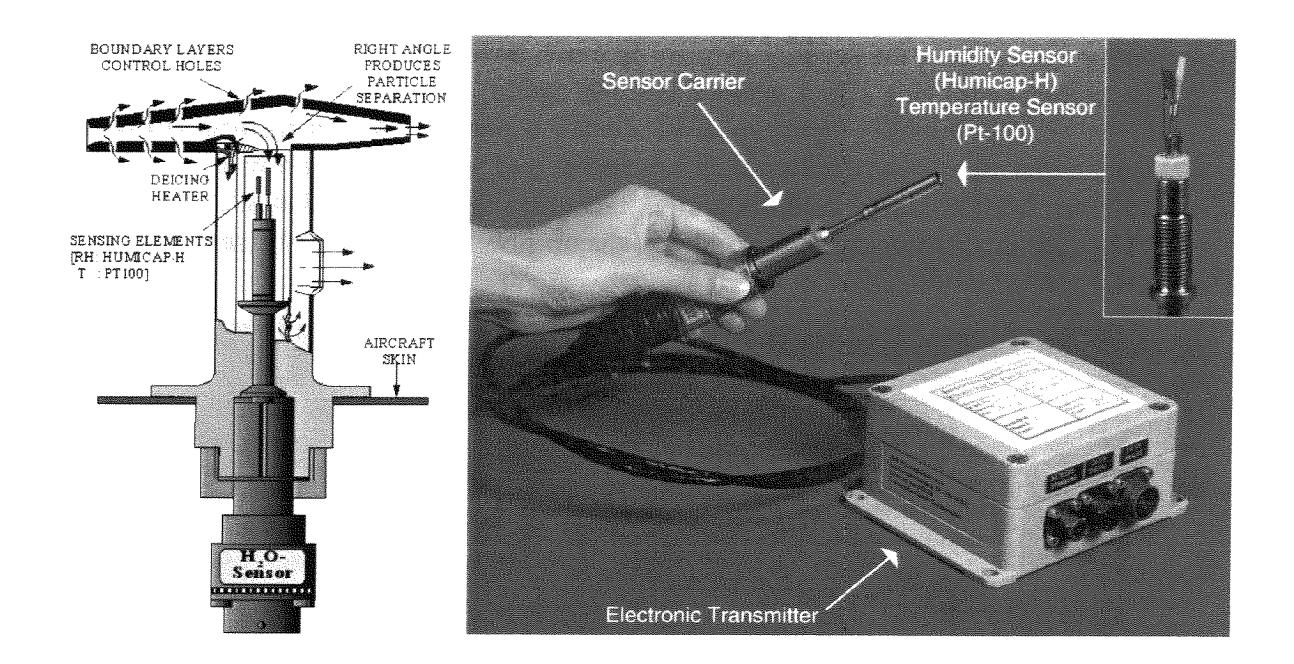


Figure 18: Left panel: Cross section of the airborne MOZAIC humidity sensor mounted in air sampling housing (Rosemount, Model 102 BX). Right panel: MOZAIC Humidity Device (MHD) to be installed in a Rosemount housing mounted on the outside skin of the Airbus A340 aircraft (see Figure 17).

#### 4.2 Calibration of MHD

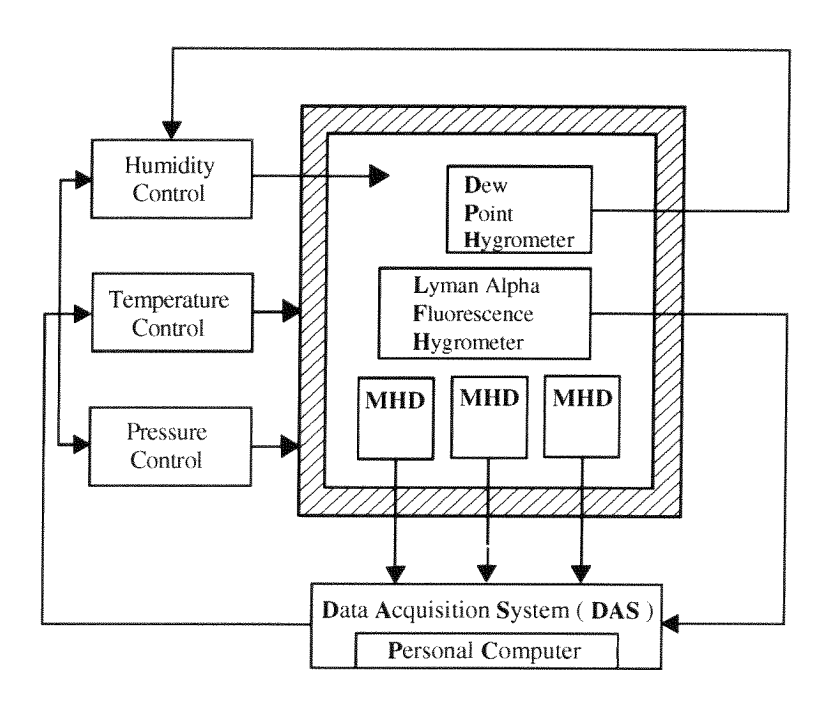


Figure 19: Scheme of the set up for the calibration of humidity sensing devices in the environmental simulation chamber

Caused by the high aircraft cruising speed of about Mach 0.8 and the strong speed reduction in the inlet part of the housing the sampled air is subject to adiabatic compression. The conversion of kinetic energy of the sampled air leads to a substantial temperature increase of about 25°C at cruise altitude (10-12 km) such that the relative

humidity measured at the sensing element is much lower than the actual relative humidity of the ambient air. This effect necessitates the careful and individual calibration of each flown MOZAIC Humidity Device against a water vapor reference instrument (LFH) in the environmental simulation facility at Jülich before and after one month of flight operation. Up to three MHDs can be calibrated simultaneously during a simulation run (See Figure 19). They are positioned just at the outlet of the air flow duct of the LFH (see Figure 20).

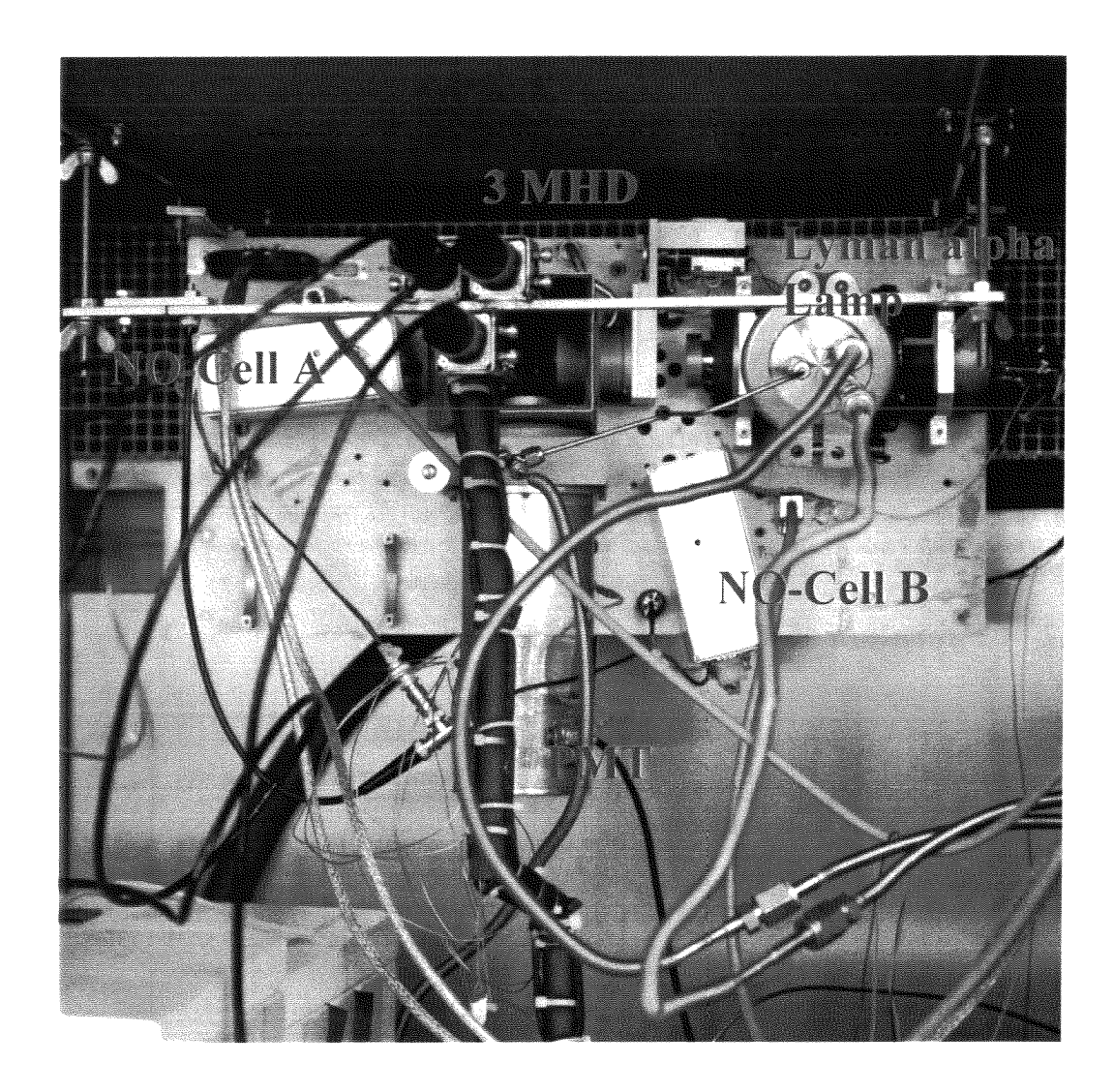
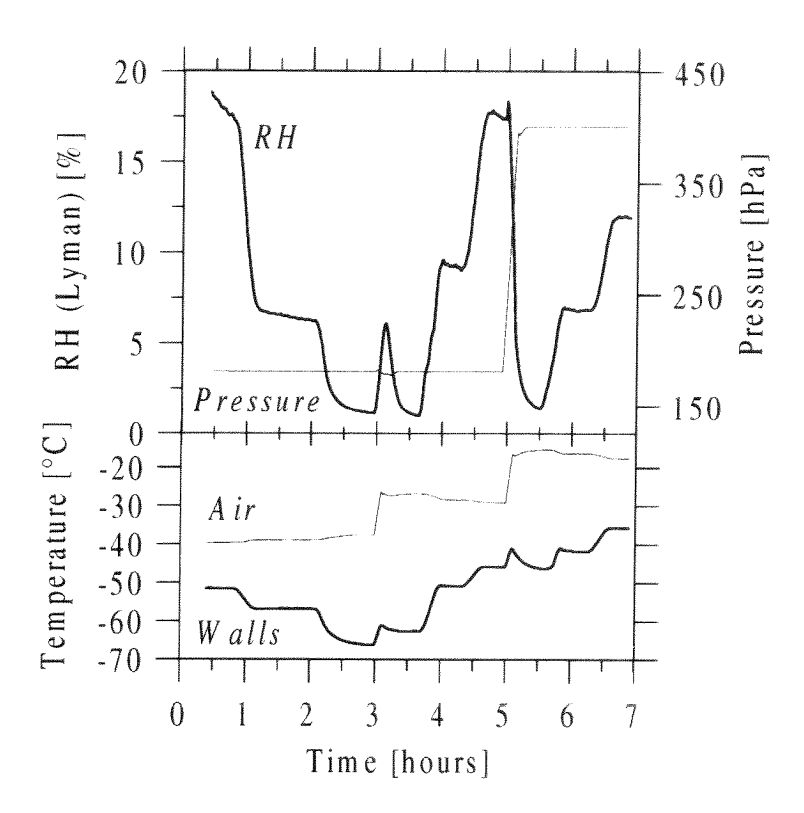


Figure 20: Three MOZAIC-Humidity Devices (MHD) installed at the outlet of the air sampling duct of the Lyman  $(\alpha)$  Fluorescence Hygrometer (LFH) in the environmental simulation chamber just prior to a calibration run (see also cross-section in Figure 8)

A typical calibration run of the chamber is shown in Figure 21. Calibration is executed at three air temperatures, -40°C, -30°C, and -20°C, the prevailing temperatures at which the humidity sensors are operating in the Rosemount housing. The pressure at -40°C and -30°C is set to 180 hPa and for -20°C changed to 400 hPa. At each temperature three different humidity levels are set by adjustment of the wall temperature to the corresponding dew point temperature while optional moistened air is added to compensate for the water deficiency effect (see section 2.6). The relatively slowly varying parts of the humidity steps are used to calibrate the MHD's with the LFH as reference.



**Figure 21**: Water vapor calibration run in the environmental simulation chamber as function of simulation time. Shown are RH, measured by Lyman-Alpha fluorescence hygrometer, pressure, air temperature, and temperature of the chamber walls.

An example of the results of a calibration of a MHD at three temperature levels is shown in Figure 22.

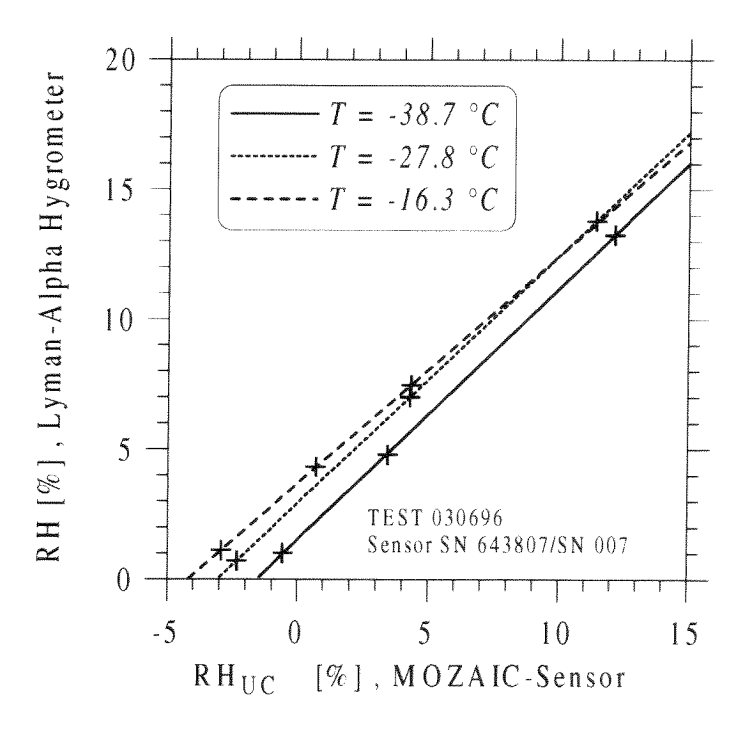


Figure 22: The calibration of a MOZAIC humidity sensor in the environmental simulation chamber results in three linear calibration curves at three different temperatures.

All calibrations revealed that the relative humidity of a calibrated sensor (RH<sub>C</sub>) for a constant temperature can be expressed by a linear relation

$$\mathbf{RH}_{\mathbf{C}} = \mathbf{a} + \mathbf{b} \cdot \mathbf{RH}_{\mathbf{UC}}, \qquad [4-1]$$

where  $RH_{UC}$  is the uncalibrated output from an individual sensor, and a and b are coefficients that result from the calibration procedure. Each calibration is executed at three temperatures,  $-20^{\circ}C$ ,  $-30^{\circ}C$ , and  $-40^{\circ}C$ , resulting in three pairs of calibration coefficients a and b.The mean of the pre- and post-flight<sup>3</sup> calibration coefficients of each flight period are used to evaluate the measurements. The differences between both sets of these calibration coefficients give the main contribution to the uncertainty of the measurement [Helten et al., 1998].

A more detailed evaluation of the calibration and performance of the MOZAIC humidity measurements is reported by *Helten et al.* [1998, 1999].

<sup>&</sup>lt;sup>3</sup> Typical time periods between pre- and post flight calibration runs are determined by the frequency of the main aircraft servicing intervalls and are roughly 500 flight hours apart.

## 5 Concluding Remarks

In a variety of simulation experiments the environmental simulation facility has demonstrated to be useful as facility for the calibration and comparison of different types of airborne ozone and humidity sensing devices used in atmospheric research.

In 1996 the environmental simulation chamber was established as World Calibration Facility for Ozone Sondes (=WCFOS) of the WMO. A first international intercomparison of eight ozone sounding laboratories from seven countries was conducted and demonstrated reliability and effectiveness of the ozone simulation in the chamber under quasi atmospheric conditions. The comparison of bare ozone sondes themselves without the accidental difficulties encountered during intercomparison field campaigns has given more clearly defined results. In collaboration with WMO in 1998 and 1999 simulation experiments were performed in preparation to the second international ozone sonde intercomparison, JOSIE-2000, to be conducted at the facility in the course of 2000.

The water vapor simulation in the environmental simulation chamber is intensively used since 1994. More than 250 calibration runs of the flown MHD's in the scope of the MOZAIC program have been performed resulting in clearly defined knowledge about the instrumental performance of the MHD and the accuracy of the water vapor measurements made in MOZAIC. Evaluation of two years of MHD-calibrations have shown that an accuracy of ±5% relative humidity between ground and 12 km altitude is achieved (Helten et al., 1998). During normal flight operation the accuracy of the MHD has been checked and confirmed through in-flight comparison with reference instrumentation [Helten et al., 1999].

Further, the facility is a platform to characterize humidity sensors deployed on radiosondes as well as to investigate the performance of new developed airborne sensing devices.

## **Acknowledgment**

We acknowledge with gratitude Mike Proffitt and the NOAA Aeronomy Laboratory for supplying the balloon borne UV-absorption photometer as the ozone reference of the facility. The development of the facility to simulate ozone soundings was supported partially by the German Minister for Research and Technology (BMFT) under grant no. 07 EU 723. Chamber adaptions to test new types of ozone sondes were funded by the European Commission (DG-XII-D: Environmental Program) within the scope of the NOZES-project. The instrumental development and adaptation of the facility to calibrate water vapor sensing devices in the scope of the MOZAIC I and II projects were funded by the European Commission, DG XII-C: Aeronautics and DG XII-D: Environmental Program, respectively.

#### References

Attmannspacher, W. and H. Dütsch, International Ozone Sonde Intercomparison at the Observatory of Hohenpeissenberg, *Berichte des Deutschen Wetterdienstes*, 120, 1970.

Attmannspacher, W. and H. Dütsch, 2nd International Ozone Sonde Intercomparison at the Observatory of Hohenpeissenberg, *Berichte des Deutschen Wetterdienstes*, 157, 1981.

Global Atmosphere Watch Guide, GAW-Report No. 86, WMO/TD-No. 553, World Meteorological Organization, Geneva, 1993.

Goff, J.A., and Gratch, S., Low-pressure properties of water from -160 to 212 F, *Trans. Amer. Soc. Heat. Vent. Eng.*, 52, 95-122, 1946.

Helten, M., H.G.J. Smit, W. Sträter, D. Kley, P. Nedelec, M. Zöger, and R. Busen, Calibration and Performance of Automatic Compact Intrumentation for the Measurement of Relative Humidity from Passenger Aircraft. *J. Geophys. Res.* 103, 25643 - 25652, 1998.

Helten, M., H.G.J. Smit, D. Kley, J. Ovarlez, H. Schlager, R. Baumann, U. Schumann, P. Nedelec, A. Marenco, In-flight intercomparison of MOZAIC and POLINAT water vapor Measurements, *J. Geophys. Res.*, 104, 26,087-26,096, 1999.

Hilsenrath, E., W. Attmannspacher, A. Bass, W. Evans, R. Hagemeyer, R.A. Barnes, W.Komhyr, K. Mauersberger, J. Mentall, M. Profitt, D. Robbins, S. Taylor, A. Torres and E. Weinstock, Results from the Balloon Ozone Intercomparison Campaign (BOIC), *J. Geophys.Res.* 91, 13137-13152, 1986.

IPPC (=Intergovernmental Panel on Climate Change), Climate Change 1994: Radiative Forcing of Climate Change and An Evaluation of the IPCC IS92 Emissions Scenarios, Report of working groups 11 and 111 of the Intergovernmental Panel on Climate Change, Cambridge University Press, 1995.

Kerr, J.B., H.Fast, C.T. McElroy, S.J. Oltmans, J.A. Lathrop, E. Kyro, A. Paukkunen, H. Claude, U. Köhler, C.R. Sreedharan, T. Takao, and Y., Tsukagoshi, The 1991 WMO International Ozone Sonde Intercomparison at Vanscoy, Canada, *Atm. Ocean*, *32*, 685-716, 1994.

Kley, D. and Stone, E.J., Measurement of water vapor in the stratosphere by photodissociation with Ly (α) (1216 A) light, *Rev. Sci. Instrum.*, 49, 691-697, 1978.

Kley, D., Stone, E.J., Henderson, W.R., Drummond, J.W., Harrop, W.J., Schmeltekopf, A.L., Thompson, T.L., and Winkler, R.H., In Situ Measurements of the Mixing Ratio of Water Vapor in the Stratosphere, *J. Atm. Sci.* 36, 2513-2524, 1979.

Kley, D., Ly ( $\alpha$ ) absorption cross-section of H<sub>2</sub>O and O<sub>2</sub>, J. Atm. Chem., 2, 203-210, 1984.

Kley, D., P.J. Crutzen, H.G.J. Smit, H. Vömel, S.J. Oltmans, H. Grassl, and V. Ramanathan, Observations of near-zero ozone levels over the convective Pacific: Effects on air chemistry, *Science*, 274, 230-233, 1996.

Komhyr, W.D., Electrochemical concentration cells for gas analysis, *Ann. Geoph.*, 25, 203-210, 1969.

Levich, V.G., Physicochemical Hydrodynamics, *Prentice-Hall, Englewood Cliffs, NJ*, 1962.

Proffitt, M.H., and R.J. McLaughlin, Fast response dual-beam UV-absorption photometer suitable for use on stratospheric balloons, *Rev. Sci. Instrum.*, *54*, 1719-1728, 1983.

Ramanathan, V., R.J. Cicerone, H.B. Singh and J.T. Kiehl, Trace gas trends and their potential role in climate change, *J. Geophys. Res.*, 90, 5547-5566, 1985.

Smit, H.G.J., W. Sträter, D. Kley, and M.H. Proffitt, The evaluation of ECC-ozone sondes under quasi flight conditions in the environmental simulation chamber at Jülich, *in P.M. Borell et al. (eds.), Proceedings of Eurotrac symposium 1994, 349-353, SPB Academic Publishing by, The Hague, The Netherlands*, 1994.

Smit H.G.J., W. Sträter, M. Helten, D. Kley, D. Ciupa, H.J. Claude, U. Köhler, B. Hoegger, G. Levrat, B. Johnson, S.J. Oltmans, J.B. Kerr, D.W. Tarasick, J. Davies, M. Shitamichi, S.K. Srivastav, C. Vialle, and G. Velghe, JOSIE: The 1996 WMO International intercomparison of ozone sondes under quasi flight conditions in the environmental simulation chamber at Jülich, *Proceedings of the XVIII Quadrennial Ozone Symposium, Eds. R. Bojkov*, and G. Visconti, L'Aquila, Italy, September 1996, 971-974, 1998-A.

Smit, H.G.J., and D. Kley, Jülich Ozone Sonde Intercomparison Experiment (JOSIE), WMO Global Atmosphere Watch report series, No. 130 (Technical Document No. 926), World Meteorological Organization, Geneva, 1998-B.

Sonntag, D., Advancements in the field of hygrometry, *Meteorol. Zeitschrift, N.F. 3*, 51-66, 1994.

SPARC-IOC-GAW Assessment of Trends in the Vertical Distribution of Ozone, SPARC report No.1, WMO Global Ozone Research and Monitoring Project Report No. 43, 1998.

Thompson, A.M., The oxidizing capacity of the earth's atmosphere: Probably past and future changes, *Science*, 256, 1157-1165, 1992.

U.S. Standard Atmosphere, NOAA, NASA, USAF, U.S. Government Printing Office, Washington, D.C., 1976.

Vigroux, E., Determination des coefficients moyen d'absorption de l'ozone, *Ann. Phys.*, 8, 709-762, 1953.

WMO-Report No.8, Measurement of atmospheric humidity, Guide to meteorological instruments and methods of observation., 5<sup>th</sup> ed., *World Meteorological Organization*, *Geneva*, 5.1-5.19, 1983.

WMO report No. 104, Report of the fourth WMO meeting of experts on the quality assurance/science activity centers (QA/SACs) of the global atmosphere watch. Jointly held with the first meeting of the coordinating committees of IGAC-GLONET and IGAC-ACE at Garmisch-Partenkirchen, Germany, 13-17 March 1995, WMO TD.No. 689, World Meteorological Organization, Geneva, 1995

WMO (=World Meteorological Organization), Scientific Assessment of Ozone Depletion: 1998, Global Ozone Research and Monitoring Project - Report No. 44, World Meteorological Organization, Geneva, 1999.

			THE THE PROPERTY OF THE PROPER
			PART POT THE RESIDENCE PROPERTY OF THE PART OF THE PAR
			мониция и потерия по потерия и поте
			writelesisisisisisteennistuudaluutuutuu
			986

# Forschungszentrum Jülich



Jül-3796 July 2000 ISSN 0944-2952

